JCI The Journal of Clinical Investigation

# Spatially distinct tumor immune microenvironments stratify triple-negative breast cancers

Tina Gruosso, … , Benjamin Haibe-Kains, Morag Park

*J Clin Invest.* 2019. https://doi.org/10.1172/JCI96313.

**Research** In-Press Preview **Oncology**

Understanding the tumor immune microenvironment (TIME) promises to be key for optimal cancer therapy, especially in triple-negative breast cancer (TNBC). Integrating spatial resolution of immune cells with laser capture microdissection gene expression profiles, we defined distinct TIME stratification in TNBC with implications for current therapies, including immune checkpoint blockade. TNBCs with an immunoreactive microenvironment exhibited tumoral infiltration of granzyme B$^+$ CD8$^+$ T cells, a type I interferon signature, elevated expression of multiple immune inhibitory molecules, including IDO, PD-L1, and good outcome. An “immune-cold” microenvironment with absence of tumoral CD8$^+$ T cells was defined by elevated expression of the immunosuppressive marker B7-H4, signatures of fibrotic stroma and poor outcome. A distinct poor outcome immunomodulatory microenvironment, hitherto poorly characterized, exhibited stromal restriction of CD8$^+$ T cells, stromal expression of PD-L1 and enrichment for signatures of cholesterol biosynthesis. Metasignatures defining these TIME subtypes stratified TNBC, predicting outcome and identifying potential therapeutic targets for TNBC.



# Spatially distinct tumor immune microenvironments stratify Triple Negative Breast Cancers

Tina Gruosso[1,2], Mathieu Gigoux[1*], Venkata Satya Kumar Manem[3,4*], Nicholas Bertos[1*], Dongmei Zuo[1], Irina Perlitch[1], Sadiq Mehdi Ismail Saleh[1,5,6], Hong Zhao[1], Margarita Souleimanova[1], Radia Marie Johnson[1], Anne Monette[7], Valentina Muñoz Ramos[1], Michael Trevor Hallett[5,6,8], John Stagg[7], Réjean Lapointe[7], Atilla Omeroglu[9], Sarkis Meterissian[2,10], Laurence Buisseret[11], Gert Van den Eyden[12], Roberto Salgado[11,12], Marie-Christine Guiot[9,13], Benjamin Haibe-Kains[3,4,14,15], Morag Park[1,2,5,9]

[1]Goodman Cancer Research Centre, [2]Department of Oncology, McGill University, Montreal, Canada, [3] Princess Margaret Cancer Centre, [4]Department of Medical Biophysics, University of Toronto, Toronto, Ontario, Canada, [5]Department of Biochemistry, [6]Centre for Bioinformatics, McGill University, Montreal, Canada, [7]Centre de Recherche du Centre Hospitalier de l'Université de Montréal et Institut du Cancer de Montréal, Montréal, Canada, [8]School of Computer Science, McGill University, Montreal Canada, [9]Department of Pathology, [10]Surgery, McGill University Health Centre, Montreal, Canada,[11]Breast Cancer Translational Research Laboratory, Institut Jules Bordet, Université Libre de Bruxelles, Brussels, Belgium, [12]Departments of Pathology and Cytology, GZA Hospitals, Wilrijk, Belgium, [13]Montreal Neurological Institute and Hospital, McGill University, Montreal, Canada, [14]Department of

Computer Science, University of Toronto, Toronto, Ontario, Canada, [15]Ontario Institute of Cancer Research, Toronto, Ontario, Canada.

[*]Equal contribution

**Corresponding author**

Correspondence should be addressed to Morag Park (morag.park@mcgill.ca),

3649 Prom. Sir William Osler, GCRC Room 514, Montréal, Québec H3G 0B1, Canada.

Phone: +1 514 398 5749. Fax: +1 514 398 6769

**Conflict of interest**

JS is a permanent member of the Scientific Advisory Board and holds stocks of Surface Oncology. The other authors declare no potential conflicts of interest.

**ABSTRACT**

Understanding the tumor immune microenvironment (TIME) promises to be key for optimal cancer therapy, especially in triple-negative breast cancer (TNBC). Integrating spatial resolution of immune cells with laser capture microdissection gene expression profiles, we defined distinct TIME stratification in TNBC with implications for current therapies, including immune checkpoint blockade. TNBCs with an immunoreactive microenvironment exhibited tumoral infiltration of granzyme $B^+$ $CD8^+$ T cells, a type I interferon signature, elevated expression of multiple immune inhibitory molecules, including IDO, PD-L1, and good outcome. An "immune-cold" microenvironment with absence of tumoral $CD8^+$ T cells was defined by elevated expression of the immunosuppressive marker B7-H4, signatures of fibrotic stroma and poor outcome. A distinct poor outcome immunomodulatory microenvironment, hitherto poorly characterized, exhibited stromal restriction of $CD8^+$ T cells, stromal expression of PD-L1 and enrichment for signatures of cholesterol biosynthesis. Metasignatures defining these TIME subtypes stratified TNBC, predict outcome and identify potential therapeutic targets for TNBC.

## INTRODUCTION

Triple-negative breast cancer (TNBC) lacks targeted therapies, has high rates of distant recurrence and poor overall survival. Large-scale gene expression and sequencing studies have revealed high heterogeneity within the TNBC subtype and few common actionable targets (1-5). Despite overall poor outcome, a subset of TNBC patients respond well to standard-of-care chemotherapy, implying the existence of distinct TNBC phenotypes. However, identifying those patients most likely to respond to therapy remains an important clinical challenge.

Increasing evidence indicates that interactions between tumor cells, tumor stroma and the tumor immune microenvironment (TIME) evolve during the course of disease and play a key role in response to therapies (6). Some tumors evade immune control, enabling tumor progression. Others are subject to immune attack mediated by the establishment of a helper T cell type I response which can be subsequently modulated through expression of immunomodulatory ligands (7, 8). Such heterogeneity in the TIME and its evolution throughout tumor progression is still poorly understood.

Importantly, the presence and localization of tumor infiltrating lymphocytes (TILs) correlates with better prognosis and with improved response to neoadjuvant chemotherapy in TNBC (9, 10). This understanding has led to the development of guidelines for TIL scoring to harmonize TIL evaluation in breast cancer. However, these guidelines do not elaborate on the importance of TIL location. While stromal TILs (sTILs) constitute the most reproducible parameter when assessed on haematoxylin & eosin (H&E) stained sections (9), studies suggest an important role for infiltration of lymphocytes and specifically the $CD8^+$ T cells,

which represent the cytotoxic arm of the adaptive immune response, into the epithelial compartment (10, 11). This suggests that sub-localization of TILs might contribute to the prognostic and even predictive stratification of TNBC patients.

Elevated expression of the coinhibitory immune ligand PD-L1 (*CD274*) is associated with the presence of infiltrating lymphocytes (12), supporting the therapeutic value of immune modulation in the TNBC setting, through immune checkpoint blockade (ICB). However, in the setting of advanced disease, only 8 to 20% of TNBCs pre-selected for tumor or immune cell expression of PD-L1 respond to therapy targeting PD-L1 or its receptor PD-1 (13). To improve these response rates, better understanding of the various factors that influence differential lymphocyte infiltration and/or activation in TNBC is needed. In addition, there exists a paradoxical subset of patients with high expression of immune-associated signatures by gene expression studies who nevertheless experience poor outcome (14), indicating that additional complexity exists beyond the current information provided by bulk tumor immune signatures.

The tumor microenvironment (TME) plays a crucial role in tumor progression (15), including the modulation of the local immune environment (12, 16). Previous studies are limited to bulk tumor-derived expression profiles of TNBC (1-3) and can only identify an immunomodulatory subtype of TNBC associated with good outcome. Studies of bulk tumor lose information on compartment-specific signals within the tumor core and therefore do not reflect the spatial landscape of the TIME. A recent study identified heterogeneity in TIME architecture using a predetermined set of biomarkers (17). Here we identify distinct TIME subtypes, defined by spatial patterns of $CD8^+$ T cell localization and gene expression signatures in therapy-naïve TNBC tumors. By integrating spatial characterization of the immune response with gene expression profiling data from matched stromal and epithelial

tumor compartments, obtained through laser capture microdissection, we discover that each TIME is associated with distinct metasignatures of tumor microenvironment, prognosis and biomarkers. The biological processes identified that stratify and characterize each TIME subtype support the development of TIME-dependent targeted therapeutic approaches.

## RESULTS

### Distinct CD8$^+$ T cell localization profiles are observed in TNBC

To define patterns of CD8$^+$ T cell localization in TNBC, we assessed the spatial distribution of CD8$^+$ T cells in a cohort of 38 therapy-naïve TNBC by immunohistochemistry (IHC) using whole sections of formalin-fixed paraffin-embedded (FFPE) samples (**Supplemental Table 1, Supplemental Figure 1A**). For each tumor, CD8$^+$ T cell density was quantified in four distinct compartments: tumor margin (marCD8) and tumor core (corCD8), the latter collectively including tumor stroma (strCD8) and tumor epithelium (epiCD8) (**Figure 1A,B**, **Supplemental Figure 1B**). Importantly, CD8$^+$ T cell quantification in the stromal (strCD8) and epithelial (epiCD8) compartment is highly correlated with stromal and intratumoral (i.e. in the tumor epithelial compartment) TILs (sTILs and iTILs), evaluated on matched H&E stained sections as defined by the International Immuno-Oncology Biomarker Working Group (9) respectively (**Figure 1C**). This demonstrates the robustness of our CD8$^+$ T cell quantification scheme with respect to standard approaches used for clinical TIL evaluation (9).

Using the spectrum of infiltration of CD8$^+$ T cells in the different compartments, we defined TNBC subgroups according to the presence and/or differential localization of CD8$^+$ T cells referred to as TIME subtypes (**Figure 1A**, summary stratification diagram in **Figure 1D**). Tumors were first divided by corCD8 into corCD8$^{high}$ and corCD8$^{low}$. The majority of the corCD8$^{low}$ group demonstrated accumulation of CD8$^+$ T cells at tumor margins (marCD8$^{high}$) and were designated “Margin restricted” (MR) (12/16), while a few tumors (4/16) displayed low abundance of CD8$^+$ T cells at margins (marCD8$^{low}$) and were defined as “Immune desert”

(ID) (**Figure 1A,B,D, Supplemental Figure 2**). Alternatively, corCD8$^{high}$ tumors (22) were divided into two subgroups, with "Fully inflamed" (FI) (11/22) tumors exhibiting significant CD8$^{+}$ T cell infiltration into the tumor epithelial compartment (epiCD8$^{high}$) in addition to their presence in the stroma, while "Stroma restricted" (SR) (11/22) tumors exhibited accumulation of CD8$^{+}$ T cells in the stroma (strCD8$^{high}$) with exclusion from the tumor epithelial compartment (epiCD8$^{low}$) (**Figure 1A,B,D, Supplemental Figure 2**).

No significant differences in clinical variables, including tumor size, grade and lymph node status, were observed between these groups (**Supplemental Table 1**). Based on gene expression profiling of matched bulk tumor specimens (n=37), 31 of the 37 TNBC samples in this dataset belong to the PAM50-defined basal-like subtype (5) (**Figure 2A**). Consistent with the TNBC subtypes (TNBCTypes) defined by Lehmann *et al.* (1), corCD8$^{high}$ tumors are significantly enriched in the Immunomodulatory (IM) subtype of TNBC. In contrast corCD8$^{low}$ tumors are significantly enriched in the Mesenchymal (M) subtype (**Figure 2B-D**).

**Metasignatures derived from immune microenvironments reflect different biologies**

To assess whether specific biological processes are linked to differential CD8$^{+}$ T cell localization, we profiled gene expression in matched samples derived from bulk tumor (n=37) and tumor stromal and epithelial compartments, isolated by laser capture microdissection (LCM) (n=38) (Bulk: GSE88847; LCM: GSE88715). To understand the contributions of stromal and epithelial compartments to the biological differences between the TIME-based TNBC subgroups identified, GSEA-based Metasignatures (MSigs), derived from bulk tumor gene expression data, were used to interrogate LCM-derived tumor stromal and epithelial

gene expression datasets (**Figure 3**). Through this analysis we were able to decipher more precisely the source of the various biological pathways identified (**Figure 4**).

To identify pathways associated with each specific pattern of $CD8^+$ T cell localization, we followed a two-step classification scheme (**Figure 1D**). We first identified pathways differing between $corCD8^{high}$ (SR and FI) and $corCD8^{low}$ (ID and MR) tumors, by clustering all significant pathways correlated (positively or inversely) with corCD8 (FDR<5%). Clustering analysis of pathway enrichments identified four metasignatures (corCD8 MSigs; **Figure 3B, Figure 4A**; **Supplemental Table 2**). As expected, the predominant metasignature enriched in $corCD8^{high}$ bulk tumors reflected elevated immune signaling (corCD8 MSig1; "Immune") (**Figure 3B, Figure 4A; Supplemental Table 2**). These pathways were equally enriched in both the tumor stroma and the tumor epithelium compartments (**Figure 3B, Figure 4A; Supplemental Table 2**), consistent with the distribution of $CD8^+$ T cells within the tissue. By contrast, the predominant metasignature associated with $corCD8^{low}$ bulk tumors included fibrosis and matrix remodeling pathways (corCD8 MSig 3; "Fibrosis") (**Figure 3B, Figure 4A, Supplemental Table 2**). Consistent with signatures of reactive stroma, we observed that $corCD8^{low}$ tumors are enriched in fibrotic foci (**Figure 5**), defined as scar-like areas associated with reactive tumor stroma and poor prognosis (18). Moreover, signaling pathways linked to TGFβ, a key regulator of fibrosis, are enriched in the tumor stroma of $corCD8^{low}$ tumors (**Supplemental Figure 3**). Accordingly, $corCD8^{low}$ tumors are enriched for the "mesenchymal" Lehmann TNBC subtype (**Figure 2B,C**). This subtype is characterized by ECM receptor interaction, as well as actin remodeling by Rho and TGFβ signaling (1). Collectively, these results support the presence of elevated reactive stroma and matrix remodeling in the poorly infiltrated $corCD8^{low}$ (ID and MR) TNBC tumors.

Within corCD8$^{high}$ tumors, we identified six metasignatures (epiCD8 MSigs) reflecting biological processes associated with epiCD8 status (**Figure 3B, Figure 4B; Supplemental Table 3**). Those enriched in FI tumors include JAK/Stat signaling (epiCD8 MSig1, "JAK/STAT"), interferon signaling and cytotoxic activity (epiCD8 MSig 2, "IFN"), and stem cell-linked transcription (epiCD8 MSig 3) (**Figure 4B; Supplemental Table 3**). In contrast, SR tumors show enrichment for signatures of mTOR signaling (epiCD8 MSig 4, "mTOR"), cholesterol biosynthesis (epiCD8 MSig 5, "Cholesterol") and IL-17 signaling (epiCD8 MSig 6) (**Figure 4B; Supplemental Table 3**). Together, these data support the association of specific patterns of CD8$^+$ T cell infiltration in SR and FI tumors with distinct tumor microenvironments.

**Fully inflamed TNBCs are characterized by a type I interferon pro-inflammatory environment.**

To identify pathways implicated in enhanced CD8$^+$ T cell recruitment into the tumor epithelium (epiCD8$^{high}$), we analyzed epithelial- and stromal-specific gene expression to find biological pathways distinguishing tumors with the FI TIME subtype from those of the SR subtype. As shown by the epiCD8 MSig2 signature (interferon signaling and cytotoxic activity), multiple pathways associated with various immune response activities are elevated in FI compared to SR tumors (**Supplemental Table 3**). This includes genes associated with a type I IFN response (e.g. *OASL*, *ISG15*), antigen presentation (e.g. *TAP*, *B2M*), cytotoxic activity (e.g. *GZMB*, *FASLG*) as well as cell death (e.g. *CASP*s and *PARP*s) (**Figure 6A,B, Supplemental Figure 4**).

Effector CD8$^+$ T cells with cytotoxic activity are distinguished by elevated expression of Granzyme B (GzmB) compared to memory CD8$^+$ T cells. To validate the presence of

cytotoxic $CD8^+$ T cells in FI tumors, we quantified GzmB staining in the tumor stroma and epithelium for our 38 patients. The density of $GzmB^+$ $CD8^+$ T cells was highest in the epithelial compartments of FI tumors while it was decreased and predominantly restricted to the stroma in SR tumors, and absent in $corCD8^{low}$ tumors (**Figure 6C-E**). These results indicate increased cytotoxic activity of $CD8^+$ T cells in FI tumors compared to SR tumors, as supported by gene expression metasignatures. Consistent with this, we observed a significant accumulation of pro-inflammatory $CD68^+$ $CD206^-$ macrophages in tumor epithelium of FI tumors when compared to the other groups (**Figure 7**) further supporting the presence of an active immune response in the epithelium of FI tumors. Together these results support a distinct anti-tumorigenic immune microenvironment, mediated by $CD8^+$ T cell cytotoxicity, in FI compared to SR TNBC.

**Stromal $CD8^+$ T cell restricted tumors display a distinct TIME.**

To determine pathways enriched in SR compared to FI tumors, we examined metasignatures specifically associated with SR tumors. One of these metasignatures (epiCD8 MSig5, **Figure 4B**) was dominated by "*Superpathway (SPP) of Cholesterol Biosynthesis*". This is the only pathway significantly inversely correlated with epiCD8 in the tumor stroma as well as bulk tumor (**Supplemental Table 3**). Accordingly, key leading edge genes involved in cholesterol biosynthesis were elevated in the SR compared to FI samples in bulk tumor (**Figure 8A,B and Supplemental Figure 5A,B**) as well as in tumor stroma (**Supplemental Figure 5C,D**) and, to a lesser extent, in tumor epithelium (**Supplemental Figure 5E,F**). Hence, compared to FI tumors, SR tumors were enriched for signatures of cholesterol biosynthesis.

Cholesterol metabolism and Type I interferon response have been shown to be inversely co-regulated (19, 20). Indeed, Type I interferon signaling, reflective of the SREBP2 regulated ISGs highly expressed in FI compared to SR tumors (**Figure 8C**, **Supplemental Figure 5E,H**), negatively regulates SREBP2, the transcription factor controlling expression of cholesterol biosynthesis genes (19, 20). Consistently, our data shows mutual exclusion between the cholesterol biosynthesis signature identified in SR tumors and a Type I interferon response in FI tumors (**Figure 4B, Supplemental Table 3**). These data support the idea that the observed cholesterol signature associated with exclusion of $CD8^+$ T cells from the tumor epithelium (SR tumors) is inversely related to a type I interferon signature identified in FI tumors.

A second metasignature associated with SR samples (epiCD8 MSig6) contains the "*IL-17A in psoriasis*" pathway, which is associated with autoimmunity (21) and shown to be pro-tumorigenic and immunosuppressive in cancer (22). This includes genes expressed in IL-17-producing cells and in response to IL-17, including Psoriasin (*S100A7*) (23) (**Supplemental Figure 6**). Immunofluorescence analyses reveal that SR tumors with the lowest epiCD8, exhibit higher infiltration of IL-17-producing cells than FI tumors with the highest epiCD8 profile (**Figure 8D,E, Supplemental Figure 7A**). The majority of the infiltrated IL-17 producing cells are negative for CD4 expression by immunofluorescence **(Supplemental Figure 7B-G**). Thus, enrichment of IL-17 producing cells in SR tumors is likely due to the infiltration of γδ T cells or other IL-17 producing cells. IL-17, and γδ T cells, are associated with an immunosuppressive microenvironment in part through the ability to recruit neutrophils (22, 24). In support of this, elevated levels of neutrophil-associated genes, including *AMICA1* (JAML) (**Supplemental Figure 6B**) as well as elevated levels of neutrophils are observed in

SR tumors displaying strong stromal restriction, when compared with FI tumors (**Figure 8F, Supplemental Figure 6C, 7H**). Together, these results link extreme stromal restriction of $CD8^+$ T cell within the SR TIME subtype with the presence of IL-17 producing cells and neutrophils.

Since $CD8^+$ T cells recognize antigens presented by MHC class I molecules (heterodimers composed of HLA-I and β2M subunits) via interaction with their TCR, the level of MHC-I expressed by tumor cells may influence $CD8^+$ T cell localization (25). To investigate alternative mechanisms that could determine the spatial pattern of $CD8^+$ T cell localization, we examined the level of tumoral HLA-I by immunohistochemistry, revealing that a subset of ID, MR and SR TIME subgroups contains tumors displaying loss or decreased expression of HLA-I (**Supplemental Figure 8**). In contrast, no HLA-I loss was observed in FI tumors (**Supplemental Figure 8**). Consistent positivity of all FI tumors for MHC class I, supports capacity for antigen presentation and the decreased levels of HLA class I observed in subsets of ID, MR and SR TIME subtypes may contribute to diminished infiltration of $CD8^+$ T cells in these TNBCs. While SR tumors encompass different potential immune evasion mechanisms (HLA loss, neutrophil infiltration, IL-17-producing cells infiltration) all are characterized by a high cholesterol biosynthesis signature consistent with their low interferon signature.

**Metasignatures are prognostic in an independent validation cohort**

Immune signatures can stratify TNBC patients and predict outcome (1-3), yet some patients with high expression of immune-based signatures still display poor outcome (14). Therefore, we aimed to assess the prognostic value of our metasignatures (**Figure 9**). To do so, we first identified metasignatures that best discriminate TIME subtypes in our discovery

cohort (**Figure 9**) using Cohen's kappa statistic. The corCD8 MSig1 "Immune" and corCD8 MSig3 "Fibrosis" signatures are most enriched in, and accurately predict, the corCD8$^{high}$ and the corCD8$^{low}$ tumors respectively ($\kappa$=0.55) (**Figure 4A, Figure 9B)**. Moreover, a combination of corCD8 MSig1 "Immune" and corCD8 MSig3 "Fibrosis" (referred to as "Immune/Fibrosis") displays better predictive value ($\kappa$=0.71), than either metasignature alone (**Figure 9B**). Similarly, the epiMSig2 "IFN" and epiMSig5 "Cholesterol" metasignatures are enriched in both LCM compartments and accurately predict FI and SR TIME subtypes ($\kappa$=0.45 and $\kappa$=0.46), respectively, while combining these two metasignatures (referred to as "IFN/Cholesterol") demonstrates better predictive value ($\kappa$=0.52) (**Figure 9B**).

To assess the predictive value of this two-step approach, we first applied the "Immune/Fibrosis" metasignature in an independent external dataset of chemo naïve TNBC (n=579) (3) (**Figure 9C**) for which Recurrence Free Survival (RFS) is available **(Supplemental Figure 9**). This stratifies a poor outcome Immune$^{low}$/Fibrosis$^{high}$ (MR-like) (Log-rank *P* = 0.04) and a good outcome Immune$^{high}$/Fibrosis$^{low}$ tumor subset. As a second step, the "IFN/Cholesterol" metasignature, when applied to the good outcome subset, further stratifies this subgroup into patient subsets with intermediate outcome (IFN$^{low}$/Cholesterol$^{high}$ - SR-like) and good outcome (IFN$^{high}$/Cholesterol$^{low}$ - FI-like) (Log-rank *P* = 0.04) (**Figure 9C**). Hence, stratification by sequential use of "Immune/Fibrosis" and "IFN/Cholesterol" metasignatures shows prognostic value in independent gene expression datasets derived from TNBC bulk tumor samples.

Importantly, when applied using the same two-step process (**Figure 9A,D**), both combination signatures ("Immune/Fibrosis" and "IFN/Cholesterol") have prognostic value. Thus, the corMSig1/3 "Immune/Fibrosis" combination can be used as a first step to stratify

MR-like vs. SR- and FI-like tumors. As a second step, the epiMSig 2/5 “IFN/Cholesterol” combination can then be applied to distinguish between SR-like vs. FI-like subtypes (**Figure 9D**). Together, these findings demonstrate that $CD8^+$ T cell localization pattern-derived metasignatures, when applied in a two-step approach, capture distinct aspects of TNBC patient prognosis which cannot be detected using existing approaches.

**Specific coinhibitory molecules associate with distinct immune microenvironments**

Tumors can escape immune attack using various immunosuppressive mechanisms. These include the recruitment of immunosuppressive cell types such as regulatory T ($T_{reg}$) cells as well as expression of negative regulators such as PD-1/PD-L1 that can lead to a progressive decrease in T cell effector activity and functional hyporesponsiveness (12, 26, 27). By examining gene expression, we found that multiple regulators, known to act as negative feed back loops following immune activation, are elevated in the epithelial compartment of FI tumors (**Figure 10A,B, Supplemental Figure 10**). These include members of the Ig superfamily of B7 coinhibitory receptors (*PDCD1* (PD-1)*, CTLA*, *TIGIT*) and the PD-1 ligand PD-L1 (*CD274*), as well as other checkpoint receptors including *LAG3,* TIM-3 (*HAVCR2*), and the immunoregulatory enzymes indoleamine 2,3-dioxygenase (*IDO1* and *IDO2)* (27). In contrast, expression of the B7 family members B7-H4 (*VTCN1*) and B7-H3 (*CD276)* which can mediate inhibition of T cell activity and infiltration (28, 29), are elevated in $corCD8^{low}$ (ID and MR) tumors (**Supplemental Figure 10, 11**), and are inversely correlated with *CD274* (PD-L1) (**Figure 10C, Supplementental Figure 10B**). Immunostaining supported an inverse correlation between PD-L1 and B7-H4 protein expression (**Figure 11**) as well as association with distinct TIME subgroups. Notably, PD-L1 and other markers of inflammation,

such as IDO1 are both enriched in the epithelial compartment of FI tumors and in the stromal compartment of SR tumors, but are low or absent in corCD8$^{low}$ (ID and MR) tumors (**Figure 11A,B, Supplemental Figure 12, 13**). Similarly, CD4$^{+}$ T cells that express the forkhead box P3 (FOXP3) transcription factor and can function as regulatory T ($T_{reg}$) cells are elevated in SR and FI tumors compared to MR and ID tumors and follow CD8$^{+}$ T cells, with accumulation in stroma in SR and infiltration in the epithelium compartment in FI (**Supplemental Figure 14**). Hence PD-L1 and IDO1 positivity and localization as well as FoxP3$^{+}$ CD4$^{+}$ T cells are all positively correlated with the localization pattern of CD8$^{+}$ T cells. Conversely, expression of B7-H4 is predominantly observed in the epithelial compartment of corCD8$^{low}$ (ID and MR) tumors (**Figure 11A,B**). Our results demonstrate a mutually exclusive expression of known negative regulators of T cells, PD-L1 or IDO1 as well as FoxP3 CD4$^{+}$ T cells which are positively correlated with location of CD8$^{+}$ T cells and B7-H4 which is negatively correlated with CD8$^{+}$ T cells and reveal that expression of other immune checkpoint targets is distinct between ID, MR, SR and FI TNBC tumors. These results accentuate the importance of delineating the localization of PD-L1 expression as well as that of other immune checkpoints to better understand and target mechanisms of response to immune checkpoint inhibitors and improve their efficacy.

## DISCUSSION

The immune context of TNBC has gained acceptance as an important clinical correlate, raising hopes that modulating immune responses via immunotherapies may constitute effective therapeutic strategies. However, only 8-20% of pre-selected TNBC patients benefit from anti-PD-L1 or anti-PD1 immunotherapy (13), highlighting the need for a better understanding of how the tumor and immune microenvironment (TIME) architecture influences outcome in TNBC and response to current treatment modalities (30). In this study we provide a deeper understanding of complex tumor immune microenvironments. By combining immune cell identification and localization in matched clinical samples with gene expression profiling from matched tumor epithelial and stromal compartments, we identify four distinct TIMEs (ID, MR, SR, FI) associated with disease outcome in TNBC (summarized in **Figure 12**). These are defined by distinct $CD8^+$ T cell localization patterns and harbor distinct GzmB positivity, gene expression metasignatures that predict outcome in independent whole tumor datasets, and expression of distinct patterns of immune checkpoint proteins and immunomodulatory cell types. Each TIME class represents a substantial fraction of TNBC cases, amenable for translation to patient stratification approaches. Metasignatures associated with each TIME subtype have prognostic value, provide improved stratification and support TIME-dependent therapeutic strategies for TNBC.

Our findings demonstrate that tumors with low $CD8^+$ T cells ($corCD8^{low}$, including MR and ID TIME subtypes) display poorest prognosis. These tumors are negative for expression of the immune checkpoint PD-L1, immune modulator IDO1 and display elevated signatures of

fibrosis and fibrotic foci. Similar signatures characterized by desmoplasia and matrix remodeling are associated with low immune content and resistance to chemotherapy in ovarian cancer (31-34). These $CD8^{low}$ TNBC tumors display elevated TGFβ-dependent signatures associated with activated stroma and immunosuppressive signals (35) as well as expression of the B7 family coinhibitory molecule, B7-H4. B7-H4 can promote an immunosuppressive environment by negatively regulating T cell effector function and infiltration (28, 36, 37). Although originally characterized by its expression on haematopoietic cells, elevated levels of B7-H4 on tumor cells, such as observed here, correlate with poor clinical outcome across multiple solid tumors (38). Consistent with our data, B7-H4 expression is upregulated by TGF-β1 signalling in colorectal cancer (39). Notably for poor outcome TNBC, expression of B7-H4 is inversely correlated with PD-L1 protein and signatures of inflammation indicating that, in these TNBC, B7-H4 may actively suppress immune infiltration. A similar inverse correlation between B7-H4 and PD-L1 was described in lung carcinoma (40). This indicates the utility of B7-H4 as a biomarker for "immune-cold" tumors and as a potential target for TNBC and other PD-L1 negative solid tumors that display low infiltration of $CD8^+$ T cells and raises the potential use of inhibitors of TGF-β1 signalling to sensitize immune cold tumors to PD-1/PD-L1 immunotherapy (41).

In contrast, the fully infiltrated (FI) TIME TNBC subtype displays a pro-inflammatory microenvironment defined by a type I IFN gene signature, the presence of $GzmB^+$ $CD8^+$ T cells and proinflammatory $CD68^+$ $CD206^-$ macrophages in the tumor epithelium, as well as good outcome. This supports previous studies showing that elevated immune infiltration (10, 42, 43) and immune signatures (1-3) predict good outcome and response to chemotherapies. Although the FI TIME TNBC subtype displays good outcome, it possesses the highest gene

expression levels of several immune checkpoints (e.g. Lag-3, Tim-3, TIGIT, CTLA-4 and PD-L1) as well as positivity for PD-L1, IDO1 and elevated infiltration of $FoxP3^+$ $CD4^+$ T cells in the tumor epithelium compartment. This likely reflects negative feedback consistent with the proinflammatory nature of these tumors and supports the selection of these cases as candidates for immunotherapeutic strategies (12, 44). Such negative feedback may be selected for during the progression from breast ductal carcinoma *in situ* (DCIS) to invasive ductal carcinoma (IDC) (45).

Using our compartment-specific analysis, we have identified a unique TIME characterized by $CD8^+$ T cell accumulation in the stroma (Stroma restricted, SR TIME). These patients experience poorer overall survival in large independent breast cancer cohorts (10), yet factors contributing to this are poorly described. SR tumors with highest accumulation of $CD8^+$ T cells in tumor stroma exhibit elevated IL-17-producing $CD4^-$ $\gamma\delta$T cells as well as neutrophils when compared to FI TIME tumors. IL-17 producing $\gamma\delta$T cells are associated with recruitment of neutrophils with pro-tumorigenic activities and tumor progression (22, 24). In SR tumors, the stroma, but not epithelium, compartment displays positivity for PD-L1, IDO1 as well as $FoxP3^+$ $CD4^+$ T cell infiltration, supporting the development of a potentially immunosuppressive stromal microenvironment. In this context, macrophages in peritumoral stroma can foster immune privilege and disease progression through expression of PD-L1 (46).

In many solid tumors, clinical responses to anti-PD-L1/PD-1 therapy occur most often in patients with tumors identified as inflamed (12). Clinical trials using PD-1/PD-L1 immune checkpoints inhibitors show response in up to 8-20% of $PD\text{-}L1^+$ TNBCs in advanced settings (13). Although FI TIME tumors that harbor PD-L1 expression in the tumor epithelial

compartment, may be expected to derive the greatest benefit from immune checkpoint blockade therapies, our study and others indicate that FI TNBC patients have the best outcome of TNBC on standard-of-care chemotherapies (12). Hence, FI TNBC patients may not be well represented in most of the anti-PD-1/PD-L1 clinical trial cohorts of advanced disease and may be a patient population suitable for immune checkpoint therapies in the neoadjuvant or adjuvant setting.

Selection of patients for anti-PD-1/PD-L1 therapies is based on PD-L1 protein positivity (47) regardless of its spatial localization. However, PD-L1 expression has been shown to be enriched in tumor cells or immune cells in distinct TNBC (17). Our study highlights the importance of stromal PD-L1 positivity in SR TNBC patients, raising the possibility that these patients may respond differently to anti-PD-L1 therapies. In addition, although PD-L1 positivity by IHC enriches for populations with clinical benefit, PD-L1 testing alone is not sufficient to accurately predict response to immune checkpoint blockade therapy (48). Hence, further analysis of spatial expression patterns of immune checkpoint biomarkers (including PD-L1 but also B7-H4, IDO1 and others) is critical to assess the predictive value, clinical relevance and optimal combinations of such biomarkers and improve patient stratification for clinical trials of immune checkpoint therapies.

In our study, the identification of the SR TIME subtype, an immune signature subtype with poorer outcome in TNBC (10), demonstrates the importance of including the spatial pattern of $CD8^+$ T cell localization when characterizing TNBC subgroups. Clinically, SR tumors that display accumulation of $CD8^+$ T cells in the tumor stroma would be scored as “immune-positive” using current pathology guidelines. This includes the “Immunoscore” for bulk immune infiltration (49), or current guidelines for TIL assessment, where stromal TILs

(sTILs) are preferentially scored (9). Hence using the current guidelines, SR tumors would not be fully distinguished from FI tumors, despite their association with poorer prognosis (10) and that these subtypes are expected to respond differently to therapies.

Currently, bulk gene expression analyses have failed to integrate spatial information of immune cells and do not accurately predict the TIME subtypes identified here (1-3). Using data from bulk tumors, our patients with the SR TIME subtype displayed elevated levels of "pan-immune" signatures shown by some studies to be predictive of good outcome (10, 14). Supporting this, the Lehmann immunomodulatory subtype, derived using bulk tumor, was unable to differentiate between FI and SR TNBC. In contrast, our Metasignatures, derived from gene expression analysis of matched tumor stroma and tumor epithelium with additional stratification based on $CD8^+$ T cell localization, allow discrimination between SR and FI tumors. Moreover, our data show that the inverse correlation of Cholesterol biosynthesis and Type 1 Interferon signatures can distinguish TNBCs with FI and SR TIME subtypes, providing an approach to identify the SR TIME subtype TNBC in bulk tumor retrospective datasets. This is consistent with reciprocal negative regulation of the cholesterol and interferon pathways following viral infection, whereby the cholesterol biosynthesis pathway (low in FI TNBC) is transcriptionally downregulated by type 1 interferon signalling (19, 20, 50), characteristic of FI tumors. Hence the decrease of the cholesterol biosynthesis signature in FI versus SR tumors is consistent with enhanced type 1 interferon signatures in FI tumors over SR tumors (**Figure 6A,B**). In support of a negative feedback loop between the interferon and cholesterol biosynthesis pathways, the combination of "IFN/Cholesterol" metasignatures (epiMSigs 2/5) more accurately predicts the SR and FI subtypes in our cohort and shows better prognostic value over using either metasignature alone in independent datasets of bulk tumors. From our

work, the prognostic value of these signatures in external gene expression datasets derived from bulk tumor TNBCs, demonstrates that TIME expression subtype and the biological processes underlying differential T cell localization, govern TNBC progression and response to standard of care therapy. Considering that SR TNBC patients display an immunosuppressive TIME with reduced Type I Interferon signalling, they may benefit from emerging vaccine-based approaches and/or IFN stimulating therapeutic strategies such as STING agonist intradelivery to enhance T cell trafficking to the tumor site (51) or demethylating agents that activate a viral mimicry and type I interferon signalling (52).

This is the first study to integrate specific spatial distribution of $CD8^+$ T cells within whole tumor sections of TNBC tumors, with compartment derived gene expression profiling, from tumor stroma and epithelium, to identify distinct TIME subtypes. TIME subtypes identified here (ID, MR, SR, FI) depict distinct immune landscapes and potential escape strategies involving differential patterns of immune checkpoint proteins (PD-L1 and B7-H4), immune modulators (IDO1), immunomodulatory cell type infiltration (macrophages, Treg, neutrophils and IL-17-producing cells), as well as HLA-I loss. These distinct spatial TIMEs could enable enhanced stratification of TNBC patients for optimal standard of care therapy as well as differential immunotherapy strategies. The approach developed here sheds light on the limitations of current TNBC stratifications, immune infiltration assessments and the use of bulk tumor gene expression datasets, all of which fail to fully integrate the heterogeneity of $CD8^+$ T cell spatial distribution and the distinct underlying biologies. A better understanding of the TIME subtypes identified here will contribute to our understanding of mechanisms by which TNBCs evade immune surveillance and their integration into associated clinical studies has the potential to aid in the development of new therapeutics and biomarkers.

## METHODS

### Sample collection and selection

Detailed protocols and procedures are available in supplemental methods. Samples were collected from patients undergoing breast surgeries at the McGill University Health Centre (MUHC) between 1999 and 2012. For the purposes of this study, samples were selected according to the following criteria: therapy-naïve at time of surgical excision, clinically documented lack of expression/amplification of ER, PR and HER2, a histological subtype assignment of invasive ductal carcinoma (not otherwise specified) (IDC (NOS)). Laser capture Microdissection (LCM) and gene expression profiling methodology as been previously published (15) en details in supplemental methods. Agilent Technologies SurePrint G3 Human GE 8x60K Microarrays (Cat No G4851A) were used for gene expression profiling.

### Gene expression normalization

We complemented our set of LCM samples with sample-matched bulk tumor gene expression data for 37 of 38 samples was extracted from a previously published dataset (GSE58644)(14). Loess normalization was used to correct within arrays and quantile normalization was used to correct between arrays using the R package Limma (version 3.22.7). Mean expression values were used to aggregate probes and the most variable probe was used to summarize transcripts with multiple probes mapping to it. Gene expression from stroma and epithelium were normalized separately. Raw and normalized microarray data have been deposited in the Gene Expression Omnibus database under accession numbers

GSE88715 (for the stroma and epithelium gene expression) and GSE88847 (for the bulk tumor gene expression).

**Immunohistochemistry (IHC) and immunohistofluorescence (IHF)**

IHC directed against HLA-ABC and neutrophil elastase was performed on a Ventana Benchmark XT automated system. Subsequent steps were performed as per the manufacturer's directions. Other IHC procedures were performed manually. Briefly, sections were deparaffinized, conditioned and antigens were retrieved using proprietary buffers (pH6 or pH9). After blocking, primary antibodies were applied at optimized concentrations overnight at 4°C, followed by 30 minutes of incubation with secondary HRP antibody, subsequent DAB revelation and counterstaining. For IHF, samples have been processed the same way until incubation of the primary antibody. Detection was performed with Tyramide Signal Amplification. Slides were counterstained with DAPI. Detailed staining protocols, antibodies and quantification procedures are provided in the supplemental methods.

**Pathological assessment**

Scoring of tumor infiltrating lymphocytes (TILs) and evaluation of fibrotic focus on H&E sections was performed by two trained pathologists (R.S., G.V.d.E.) who were blinded to the clinical and experimental data following the proposed guidelines for TILs in breast cancer (9) and fibrotic foci respectively (18). Details are provided in Supplemental methods.

**Grouping of patients**

All tumors with a $CD8^+$ T cell density in tumor core of < 100 cells/$mm^2$ were assigned to the $corCD8^{low}$ group compared to the $corCD8^{high}$ group. The majority of $corCD8^{low}$ group tumors show accumulation of $CD8^+$ T cells at the tumor margins (marCD8) ($corCD8^{high}$ $marCD8^{high}$) that were named Margin restricted (MR). The $corCD8^{low}$ tumor group also includes a small group of tumors with no accumulation of $CD8^+$ T cells at the tumor margins (marCD8 < 200 cells/$mm^2$) named Immune desert (ID). Tumors having a significant infiltration of $CD8^+$ T cells in the tumor core ($corCD8^{high}$) were then divided depending on the infiltration of $CD8^+$ T cells in the epithelium (epiCD8). Tumors with epiCD8 below the median (of 204.5 cells/$mm^2$) were classified as $corCD8^{high}$ $epiCD8^{low}$ and named Stroma Restricted (SR). Tumors with epiCD8 above the median were classified as $corCD8^{high}$ $epiCD8^{high}$ and named Fully Inflamed (FI).

**PAM50 and Lehmann subtyping analysis**

For PAM50 subtypes, classification of samples by PAM50 subtypes was performed using the *genefu* R package (version 1.16.0). For Lehmann subtypes, TNBC patients were labeled by "TNBCType" via the web-based tool .

**Pathway analyses, signature score and development of Metasignatures**

Pathway analyses To identify genes and pathways associated with $CD8^+$ T cell tumor core density, we first ranked all the genes on the microarray platform based on their correlation with the $CD8^+$ T cell tumor core density (corCD8) for the Bulk tumor (n=37 for bulk tumor dataset) and for tumor stroma and tumor epithelium compartment (n=38). To identify genes and pathways associated with $CD8^+$ T cell tumor epithelium density (epiCD8) in tumors infiltrated in tumor core ($corCD8^{high}$), we computed the correlation between the gene

expression profiles and epiCD8 in the set of corCD8$^{high}$ tumors (n=22) and the resulting rankings were subject to Gene Set Enrichment Analysis (GSEA) analysis. Spearman correlations were performed using R (version 3.1.3) and GSEA was performed using the *Piano* R package (version 1.12.0). Nominal *P* values obtained for each pathway were corrected for multiple testing using the false discovery approach (FDR)

Development of Metasignatures To develop whole tumor pathway-based signatures associated with the variable of interest (namely, corCD8 and epiCD8) in each patient, we used the computed GSEA analysis on our bulk tumor cohort (n=37) with pathways defined by QIAGEN's Ingenuity® Pathway Analysis (IPA®, QIAGEN Redwood City, www.qiagen.com/ingenuity). The signature score for each pathway was calculated as a signed average of the leading edge genes (the sign being defined as the sign of the correlation between the expression of the gene and the phenotype of interest) using the *sig.score* function of the *genefu* R package (version 1.16.0). Hierarchical clustering using the correlation measure as distance and complete linkage was used to cluster the pathway scores for all patients. To group highly correlated pathway-based signatures, we cut the dendrogram at a height of 0.70 to define Metasignatures (MSig) for both corCD8 and epiCD8. These MSig are associated with different biological processes as indicated by their underlying pathways.

Analysis for the enrichment of publicly available TGFβ signatures Analysis for the enrichment of publicly available TGFβ signature pathways correlated or inversely correlated with CD8$^+$ T cell core density was carried out using TGFβ signatures available from the following subsets:

chemical and genetic perturbation (C2 CGP) and oncogenic signatures (C6) from the Molecular Signature Database (MSigDB) version 4.0. (further details available in supplemental methods). To calculate the TGFβ signature score, all genes from each indicated signature represented in the corresponding heatmaps were combined. Duplicates were removed. Gene expression values were first normalized by z-score and signature scores were derived using R (version 3.1.3).

**Statistics**

Spearman correlation analyses were performed when assessing correlations. Non-parametric Mann–Whitney tests were applied when comparing between two different groups of patients as specified in figure legends. Ordinary one-way ANOVA was performed when comparing all three groups together. Statistics described above were computed using Prism GraphPad Version 6.03. Correlations in the generation of pathway analyses and signature scores were derived using R (version 3.1.3).

**Prediction by Metasignatures**

Stratifying by corCD8 then epiCD8 MSig, we first evaluated the predictive value of each metasignature in our training set (n=37). To quantify the strength of association between the metasignature and the immune groups in the discovery cohort, we used Kappa statistic for measure of agreement . The range of kappa statistic is from −1 to +1, where the value 0 represents the amount of agreement that can be expected from random chance, and +1 represents perfect agreement. The kappa values less than 0 implies that the agreement is worse than expected by chance, and indicates disagreement. In other words, the Kappa

statistic <0 indicates no agreement; 0 to 0.2 slight; 0.21 to 0.40 fair; 0.41 to 0.60 moderate; 0.61 to 0.80 substantial agreement. We performed a meta-analysis on the most biologically relevant metasignatures that represent the corCD8 and epiCD8 phenotypes. .

**Survival Analysis**

Prognostic value of gene signatures was assessed using the logrank test for Kaplan-Meier survival curves, as implemented in the *survcomp* R package. We used the Rody et al. dataset (GSE31519; n=578) (53), which is a compendium of normalized triple negative breast cancer samples, to assess the prognostic value of the gene signatures. Briefly, this compedium collected data from a single platform (Affymetrix U133A and U133 Plus 2.0 chips) and included only samples that were defined as triple negative based on the mRNA expression of ER, PgR, and HER2 status. Overall relapse-free survival was used as endpoint. We first used the combination of meta-signatures (Immune and Fibrosis) from the corCD8 to mimic the split observed in the discovery cohort, i.e. we split the TNBC patients into two groups with 60% immune$^{high}$ fibrosis$^{low}$ and 40% immune$^{low}$ fibrosis$^{high}$. We then assessed the association of the combination Metasignatures (Interferon and Cholesterol) from the epiCD8 phenotype with relapse-free survival within the immune$^{high}$ fibrosis$^{low}$ tumor sub-cohort.

**Data and code availability**

Gene expression and clinical data: Raw and normalized microarray data have been deposited in the Gene Expression Omnibus database under accession numbers GSE88715 (for the stroma and the epithelium compartment gene expression) and GSE88847 (for the bulk tumor gene expression).

Analysis code: The code and data links required to reproduce this analysis is publicly available on github.com/bhklab/EpiStromaImmune. All software dependencies are available on the Comprehensive Repository R Archive Network (CRAN) or Bioconductor (Bioconductor) . A tutorial describing how to run our analysis pipeline to generate the figures and tables is provided at the link specified above. The procedure to setup the software environment and run our analysis pipeline is also provided. This work complies with the guidelines proposed by Sandve *et al.* in terms of code availability and replicability of results.

**Study approval**

The human subject study in this manuscript was approved by the McGill University Health Centre (MUHC) review board and all patient data and biological samples were obtained from patients at MUHC after obtaining written informed consent..

## AUTHORS CONTRIBUTIONS

T.G., M.G. and M.P. participated in the conception and design of the experiments. T.G. and M.G. performed the experiments and data analysis. N.B. coordinated the use of clinical samples, supervised LCM and gene expression experiment and performed data analysis. V.S.K.M. performed metasignature generation and analysis in the external dataset. S.S. performed data normalization. D.Z. and T.G. performed IHC and IHF. I.P. participated in the IHF analysis. M.S. processed tissues and performed LCM. H.Z. performed RNA isolation and gene expression profiling. R.M.J. performed TGFβ GSVA analysis and table statistics. V.M.R. collected clinical data of the cases. M.T.H. supervised bulk tumor expression profiling. A.M., L.B., J.S. and R.L. provided expert guidance for IHF/IHC. A.O. performed pathological analyses on tissue samples before LCM. S.M.I.S. contributed to clinical analyses and tissue procurement. M.-C.G. assisted with IHC and provided expert guidance for image analysis. R.S. and G.V.d.E. performed evaluation of the samples and provided expert guidance for the pathological data analysis. B.H.-K. supervised the bioinformatics aspects of the project and contributed to manuscript preparation. M.P. initiated and supervised the tissue collection and microarray preparation. T.G., M.G, N.B. and M.P wrote the manuscript, which all authors reviewed. The authors declare no competing financial interests.

**ACKNOWLEDGMENTS**

We thank all members of the Park laboratory as well as H.W. Smith, D. Quail, G. Deblois, D. de Verteuil, C. Krawczyk, M. Ostrowski, G. Leone and P. Siegel for fruitful discussion and critical reviewing of the manuscript. We also thank A. Hellebust from Indica Labs for help with IHF analysis using HALO™ software. We are grateful to B. Calvieri (Microscopy Imaging Lab, University of Toronto) for scanning IHF slides. We thank the Histology Core Facility at the Goodman Cancer Research Centre for help with sample preparation. We thank members of the Depts of Surgery, Pathology and Anesthesia at the McGill University Health Centre for their assistance with sample collection.

This study was supported by funding from CQDM (Consortium Québécois sur la découverte du medicament/Quebec Consortium for Drug Discovery), NIH (National Institutes of Health), SU2C (Stand Up 2 Cancer, 106244.4 FC:410006066) and Merck, Sharpe & Dohme Corp./McGill Faculty of Medicine Grants for Translational Research (to M.P.). The breast tissue and data bank at McGill University is supported by funding from the Database and Tissue Bank Axis of the Réseau de Recherche en Cancer of the Fonds de Recherche du Québec-Santé and the Québec Breast Cancer Foundation (to M.P.). T.G. has been supported by the Canderel and the Charlotte and Leo Karassik Oncology fellowships.

## REFERENCES


1. Lehmann BD, Bauer JA, Chen X, Sanders ME, Chakravarthy AB, Shyr Y, and Pietenpol JA. Identification of human triple-negative breast cancer subtypes and preclinical models for selection of targeted therapies. *The Journal of clinical investigation.* 2011;121(7):2750-67.
2. Burstein MD, Tsimelzon A, Poage GM, Covington KR, Contreras A, Fuqua SA, Savage MI, Osborne CK, Hilsenbeck SG, Chang JC, et al. Comprehensive genomic analysis identifies novel subtypes and targets of triple-negative breast cancer. *Clinical cancer research : an official journal of the American Association for Cancer Research.* 2015;21(7):1688-98.
3. Rody A, Karn T, Liedtke C, Pusztai L, Ruckhaeberle E, Hanker L, Gaetje R, Solbach C, Ahr A, Metzler D, et al. A clinically relevant gene signature in triple negative and basal-like breast cancer. *Breast Cancer Res.* 2011;13(5):R97.
4. Shah SP, Roth A, Goya R, Oloumi A, Ha G, Zhao Y, Turashvili G, Ding J, Tse K, Haffari G, et al. The clonal and mutational evolution spectrum of primary triple-negative breast cancers. *Nature.* 2012;486(7403):395-9.
5. Perou CM, Sorlie T, Eisen MB, van de Rijn M, Jeffrey SS, Rees CA, Pollack JR, Ross DT, Johnsen H, Akslen LA, et al. Molecular portraits of human breast tumours. *Nature.* 2000;406(6797):747-52.
6. Binnewies M, Roberts EW, Kersten K, Chan V, Fearon DF, Merad M, Coussens LM, Gabrilovich DI, Ostrand-Rosenberg S, Hedrick CC, et al. Understanding the tumor immune microenvironment (TIME) for effective therapy. *Nature medicine.* 2018;24(5):541-50.
7. Savas P, Salgado R, Denkert C, Sotiriou C, Darcy PK, Smyth MJ, and Loi S. Clinical relevance of host immunity in breast cancer: from TILs to the clinic. *Nature reviews Clinical oncology.* 2015.
8. Ribas A. Adaptive Immune Resistance: How Cancer Protects from Immune Attack. *Cancer discovery.* 2015;5(9):915-9.
9. Salgado R, Denkert C, Demaria S, Sirtaine N, Klauschen F, Pruneri G, Wienert S, Van den Eynden G, Baehner FL, Penault-Llorca F, et al. The evaluation of tumor-infiltrating lymphocytes (TILs) in breast cancer: recommendations by an International TILs Working Group 2014. *Ann Oncol.* 2015;26(2):259-71.
10. Ali HR, Provenzano E, Dawson SJ, Blows FM, Liu B, Shah M, Earl HM, Poole CJ, Hiller L, Dunn JA, et al. Association between CD8+ T-cell infiltration and breast cancer survival in 12,439 patients. *Annals of oncology : official journal of the European Society for Medical Oncology / ESMO.* 2014;25(8):1536-43.
11. Adams S, Gray RJ, Demaria S, Goldstein L, Perez EA, Shulman LN, Martino S, Wang M, Jones VE, Saphner TJ, et al. Prognostic value of tumor-infiltrating lymphocytes in triple-negative breast cancers from two phase III randomized adjuvant breast cancer trials: ECOG 2197 and ECOG 1199. *Journal of clinical oncology : official journal of the American Society of Clinical Oncology.* 2014;32(27):2959-66.
12. Chen DS, and Mellman I. Elements of cancer immunity and the cancer-immune set point. *Nature.* 2017;541(7637):321-30.
13. Solinas C, Gombos A, Latifyan S, Piccart-Gebhart M, Kok M, and Buisseret L. Targeting immune checkpoints in breast cancer: an update of early results. *ESMO Open.* 2017;2(5):e000255.
14. Tofigh A, Suderman M, Paquet ER, Livingstone J, Bertos N, Saleh SM, Zhao H, Souleimanova M, Cory S, Lesurf R, et al. The prognostic ease and difficulty of invasive breast carcinoma. *Cell reports.* 2014;9(1):129-42.
15. Finak G, Bertos N, Pepin F, Sadekova S, Souleimanova M, Zhao H, Chen H, Omeroglu G, Meterissian S, Omeroglu A, et al. Stromal gene expression predicts clinical outcome in breast cancer. *Nature medicine.* 2008;14(5):518-27.
16. Joyce JA, and Fearon DT. T cell exclusion, immune privilege, and the tumor microenvironment. *Science.* 2015;348(6230):74-80.

17. Keren L, Bosse M, Marquez D, Angoshtari R, Jain S, Varma S, Yang SR, Kurian A, Van Valen D, West R, et al. A Structured Tumor-Immune Microenvironment in Triple Negative Breast Cancer Revealed by Multiplexed Ion Beam Imaging. *Cell.* 2018;174(6):1373-87 e19.
18. Van den Eynden GG, Colpaert CG, Couvelard A, Pezzella F, Dirix LY, Vermeulen PB, Van Marck EA, and Hasebe T. A fibrotic focus is a prognostic factor and a surrogate marker for hypoxia and (lymph)angiogenesis in breast cancer: review of the literature and proposal on the criteria of evaluation. *Histopathology.* 2007;51(4):440-51.
19. Blanc M, Hsieh WY, Robertson KA, Kropp KA, Forster T, Shui G, Lacaze P, Watterson S, Griffiths SJ, Spann NJ, et al. The transcription factor STAT-1 couples macrophage synthesis of 25-hydroxycholesterol to the interferon antiviral response. *Immunity.* 2013;38(1):106-18.
20. Reboldi A, Dang EV, McDonald JG, Liang G, Russell DW, and Cyster JG. Inflammation. 25-Hydroxycholesterol suppresses interleukin-1-driven inflammation downstream of type I interferon. *Science.* 2014;345(6197):679-84.
21. Yang XO, Chang SH, Park H, Nurieva R, Shah B, Acero L, Wang YH, Schluns KS, Broaddus RR, Zhu Z, et al. Regulation of inflammatory responses by IL-17F. *The Journal of experimental medicine.* 2008;205(5):1063-75.
22. Coffelt SB, Kersten K, Doornebal CW, Weiden J, Vrijland K, Hau CS, Verstegen NJ, Ciampricotti M, Hawinkels LJ, Jonkers J, et al. IL-17-producing gammadelta T cells and neutrophils conspire to promote breast cancer metastasis. *Nature.* 2015;522(7556):345-8.
23. Liang SC, Tan XY, Luxenberg DP, Karim R, Dunussi-Joannopoulos K, Collins M, and Fouser LA. Interleukin (IL)-22 and IL-17 are coexpressed by Th17 cells and cooperatively enhance expression of antimicrobial peptides. *J Exp Med.* 2006;203(10):2271-9.
24. Coffelt SB, Wellenstein MD, and de Visser KE. Neutrophils in cancer: neutral no more. *Nature reviews Cancer.* 2016;16(7):431-46.
25. Garrido F, Aptsiauri N, Doorduijn EM, Garcia Lora AM, and van Hall T. The urgent need to recover MHC class I in cancers for effective immunotherapy. *Current opinion in immunology.* 2016;39(44-51.
26. Mellman I, Coukos G, and Dranoff G. Cancer immunotherapy comes of age. *Nature.* 2011;480(7378):480-9.
27. Pardoll DM. The blockade of immune checkpoints in cancer immunotherapy. *Nat Rev Cancer.* 2012;12(4):252-64.
28. Chen C, Qu QX, Shen Y, Mu CY, Zhu YB, Zhang XG, and Huang JA. Induced expression of B7-H4 on the surface of lung cancer cell by the tumor-associated macrophages: a potential mechanism of immune escape. *Cancer Lett.* 2012;317(1):99-105.
29. Ni L, and Dong C. New checkpoints in cancer immunotherapy. *Immunological reviews.* 2017;276(1):52-65.
30. Hanahan D, and Weinberg RA. Hallmarks of cancer: the next generation. *Cell.* 2011;144(5):646-74.
31. Tothill RW, Tinker AV, George J, Brown R, Fox SB, Lade S, Johnson DS, Trivett MK, Etemadmoghadam D, Locandro B, et al. Novel molecular subtypes of serous and endometrioid ovarian cancer linked to clinical outcome. *Clinical cancer research : an official journal of the American Association for Cancer Research.* 2008;14(16):5198-208.
32. Nelson BH. New insights into tumor immunity revealed by the unique genetic and genomic aspects of ovarian cancer. *Curr Opin Immunol.* 2015;33(93-100.
33. Batista L, Gruosso T, and Mechta-Grigoriou F. Ovarian cancer emerging subtypes: role of oxidative stress and fibrosis in tumour development and response to treatment. *The international journal of biochemistry & cell biology.* 2013;45(6):1092-8.
34. Mateescu B, Batista L, Cardon M, Gruosso T, de Feraudy Y, Mariani O, Nicolas A, Meyniel JP, Cottu P, Sastre-Garau X, et al. miR-141 and miR-200a act on ovarian tumorigenesis by controlling oxidative stress response. *Nature medicine.* 2011;17(12):1627-35.

35. Pickup M, Novitskiy S, and Moses HL. The roles of TGFbeta in the tumour microenvironment. *Nature reviews Cancer.* 2013;13(11):788-99.
36. Sica GL, Choi IH, Zhu G, Tamada K, Wang SD, Tamura H, Chapoval AI, Flies DB, Bajorath J, and Chen L. B7-H4, a molecule of the B7 family, negatively regulates T cell immunity. *Immunity.* 2003;18(6):849-61.
37. Prasad DV, Richards S, Mai XM, and Dong C. B7S1, a novel B7 family member that negatively regulates T cell activation. *Immunity.* 2003;18(6):863-73.
38. Song X, Shao Y, Gu W, Xu C, Mao H, Pei H, and Jiang J. Prognostic role of high B7-H4 expression in patients with solid tumors: a meta-analysis. *Oncotarget.* 2016.
39. Zhou X, Mao Y, Zhu J, Meng F, Chen Q, Tao L, Li R, Fu F, Liu C, Hu Y, et al. TGF-beta1 promotes colorectal cancer immune escape by elevating B7-H3 and B7-H4 via the miR-155/miR-143 axis. *Oncotarget.* 2016;7(41):67196-211.
40. Schalper KA, Carvajal-Hausdorf D, McLaughlin J, Altan M, Velcheti V, Gaule P, Sanmamed MF, Chen L, Herbst RS, and Rimm DL. Differential Expression and Significance of PD-L1, IDO-1, and B7-H4 in Human Lung Cancer. *Clinical cancer research : an official journal of the American Association for Cancer Research.* 2017;23(2):370-8.
41. Mariathasan S, Turley SJ, Nickles D, Castiglioni A, Yuen K, Wang Y, Kadel EE, III, Koeppen H, Astarita JL, Cubas R, et al. TGFbeta attenuates tumour response to PD-L1 blockade by contributing to exclusion of T cells. *Nature.* 2018;554(7693):544-8.
42. Dushyanthen S, Beavis PA, Savas P, Teo ZL, Zhou C, Mansour M, Darcy PK, and Loi S. Relevance of tumor-infiltrating lymphocytes in breast cancer. *BMC medicine.* 2015;13(202.
43. Savas P, Salgado R, Denkert C, Sotiriou C, Darcy PK, Smyth MJ, and Loi S. Clinical relevance of host immunity in breast cancer: from TILs to the clinic. *Nature reviews Clinical oncology.* 2016;13(4):228-41.
44. Spranger S, Spaapen RM, Zha Y, Williams J, Meng Y, Ha TT, and Gajewski TF. Up-regulation of PD-L1, IDO, and T(regs) in the melanoma tumor microenvironment is driven by CD8(+) T cells. *Science translational medicine.* 2013;5(200):200ra116.
45. Gil Del Alcazar CR, Huh SJ, Ekram MB, Trinh A, Liu LL, Beca F, Zi X, Kwak M, Bergholtz H, Su Y, et al. Immune Escape in Breast Cancer During In Situ to Invasive Carcinoma Transition. *Cancer Discov.* 2017.
46. Kuang DM, Zhao Q, Peng C, Xu J, Zhang JP, Wu C, and Zheng L. Activated monocytes in peritumoral stroma of hepatocellular carcinoma foster immune privilege and disease progression through PD-L1. *The Journal of experimental medicine.* 2009;206(6):1327-37.
47. Herbst RS, Soria JC, Kowanetz M, Fine GD, Hamid O, Gordon MS, Sosman JA, McDermott DF, Powderly JD, Gettinger SN, et al. Predictive correlates of response to the anti-PD-L1 antibody MPDL3280A in cancer patients. *Nature.* 2014;515(7528):563-7.
48. Gibney GT, Weiner LM, and Atkins MB. Predictive biomarkers for checkpoint inhibitor-based immunotherapy. *The Lancet Oncology.* 2016;17(12):e542-e51.
49. Galon J, Mlecnik B, Bindea G, Angell HK, Berger A, Lagorce C, Lugli A, Zlobec I, Hartmann A, Bifulco C, et al. Towards the introduction of the 'Immunoscore' in the classification of malignant tumours. *The Journal of pathology.* 2014;232(2):199-209.
50. York AG, Williams KJ, Argus JP, Zhou QD, Brar G, Vergnes L, Gray EE, Zhen A, Wu NC, Yamada DH, et al. Limiting Cholesterol Biosynthetic Flux Spontaneously Engages Type I IFN Signaling. *Cell.* 2015;163(7):1716-29.
51. Foote JB, Kok M, Leatherman JM, Armstrong TD, Marcinkowski BC, Ojalvo LS, Kanne DB, Jaffee EM, Dubensky TW, Jr., and Emens LA. A STING Agonist Given with OX40 Receptor and PD-L1 Modulators Primes Immunity and Reduces Tumor Growth in Tolerized Mice. *Cancer immunology research.* 2017;5(6):468-79.
52. Roulois D, Loo Yau H, Singhania R, Wang Y, Danesh A, Shen SY, Han H, Liang G, Jones PA, Pugh TJ, et al. DNA-Demethylating Agents Target Colorectal Cancer Cells by Inducing Viral Mimicry by Endogenous Transcripts. *Cell.* 2015;162(5):961-73.

53. Curtis C, Shah SP, Chin SF, Turashvili G, Rueda OM, Dunning MJ, Speed D, Lynch AG, Samarajiwa S, Yuan Y, et al. The genomic and transcriptomic architecture of 2,000 breast tumours reveals novel subgroups. *Nature.* 2012;486(7403):346-52.

# Figure 1

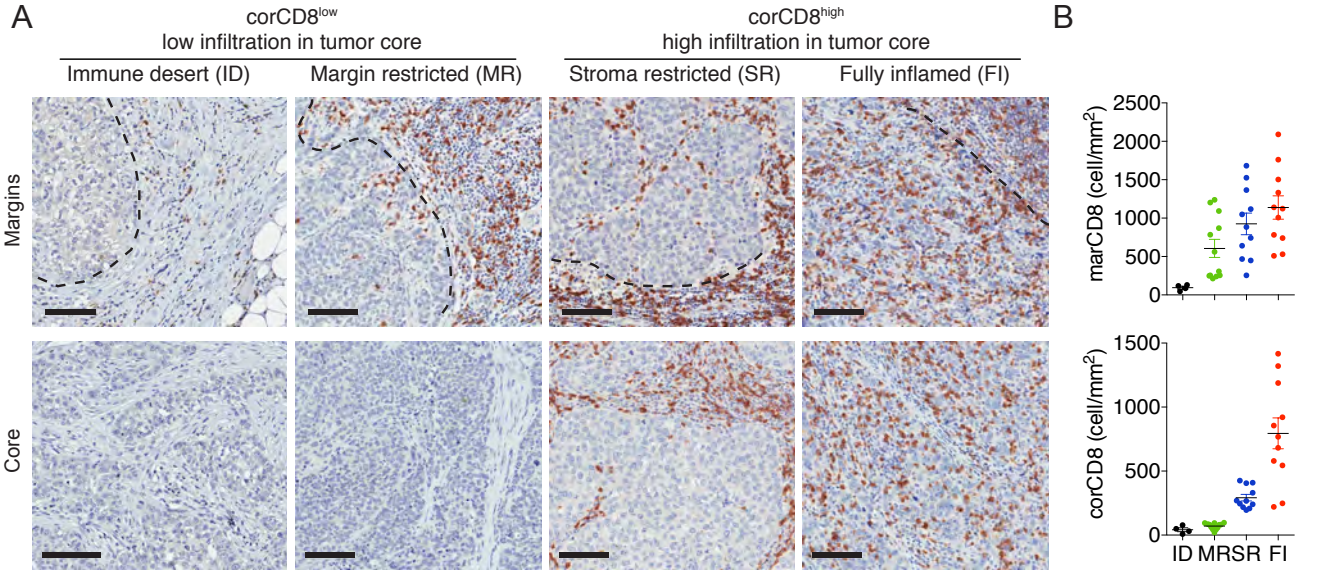


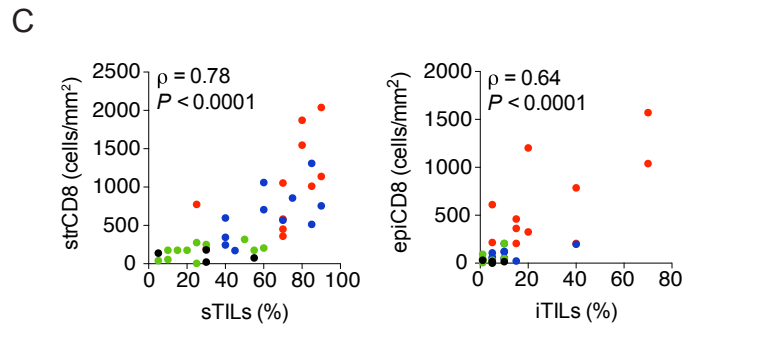


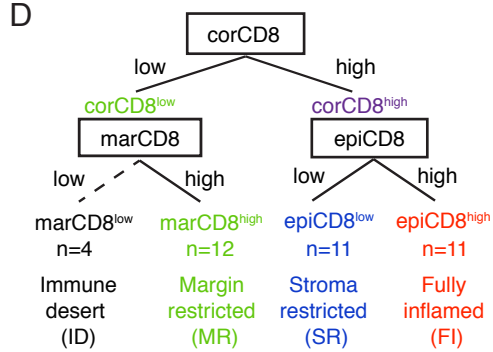


Figure 1. Therapy naïve TNBC tumors are classified into subtypes based on distinct spatial localization of CD8⁺ T cells. A) Representative images of CD8⁺ T cell staining at tumor margins (top panels; dotted line) and tumor core (bottom panels) (n=38). Scale is 100μm. B) Quantification of CD8⁺ T cell densities at tumor margins (marCD8) (top) and in the tumor core (corCD8) (bottom) (n=38). C) Comparison of strCD8 to sTILs (left) and epiCD8 to iTILs (n=38). Spearman Correlation. D) Working model of TNBC grouping based on CD8⁺ T cell localization. Black, green, blue and red represent Immune desert (ID), Margin restricted (MR), Stroma restricted (SR) and Fully inflamed (FI) tumors respectively. marCD8, corCD8, strCD8 and epiCD8 are the CD8⁺ T cell densities in the tumor margin, tumor core, tumor stroma and tumor epithelium compartment respectively. Error bars, mean ± SEM.

# Figure 2

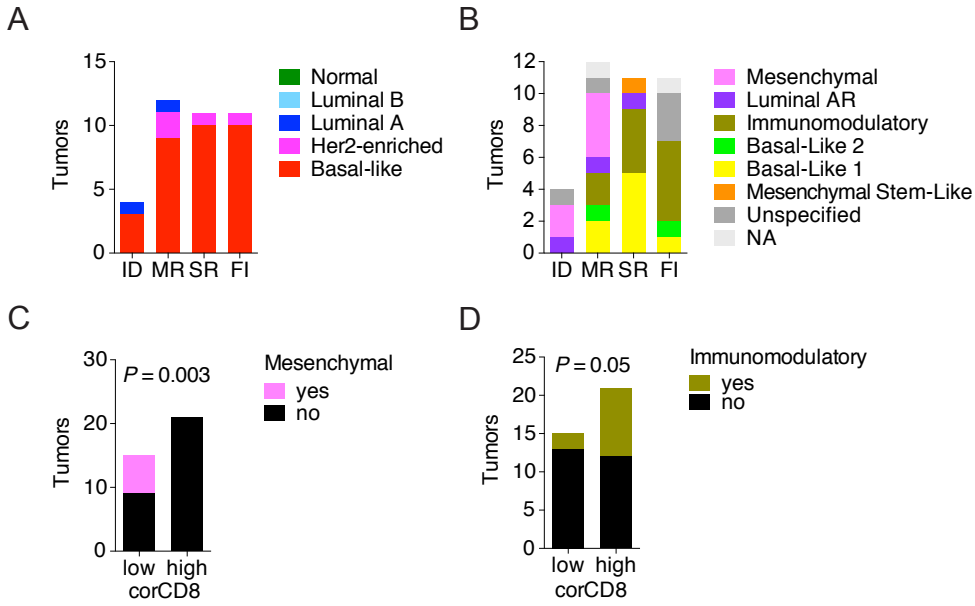


Figure 2. TIME subtypes compared to PAM50 and Lehmann breast cancer subtype stratification. A) Comparison of $CD8^+$ T cell grouping (TIME subtypes) to PAM50 molecular subtyping of our TNBC cohort (n=37). B-D) Comparison of $CD8^+$ T cell grouping (TIME subtypes) to Lehmann molecular subtyping of TNBC (n=37) showing enrichment of the mesenchymal and immunomodulatory subtypes in $corCD8^{low}$ (ID+MR), and $corCD8^{high}$ (SR+FI) respectively. Fischer Exact T test. Immune desert (ID), Margin restricted (MR), Stroma restricted (SR) and Fully inflamed (FI) tumors respectively.

# Figure 3

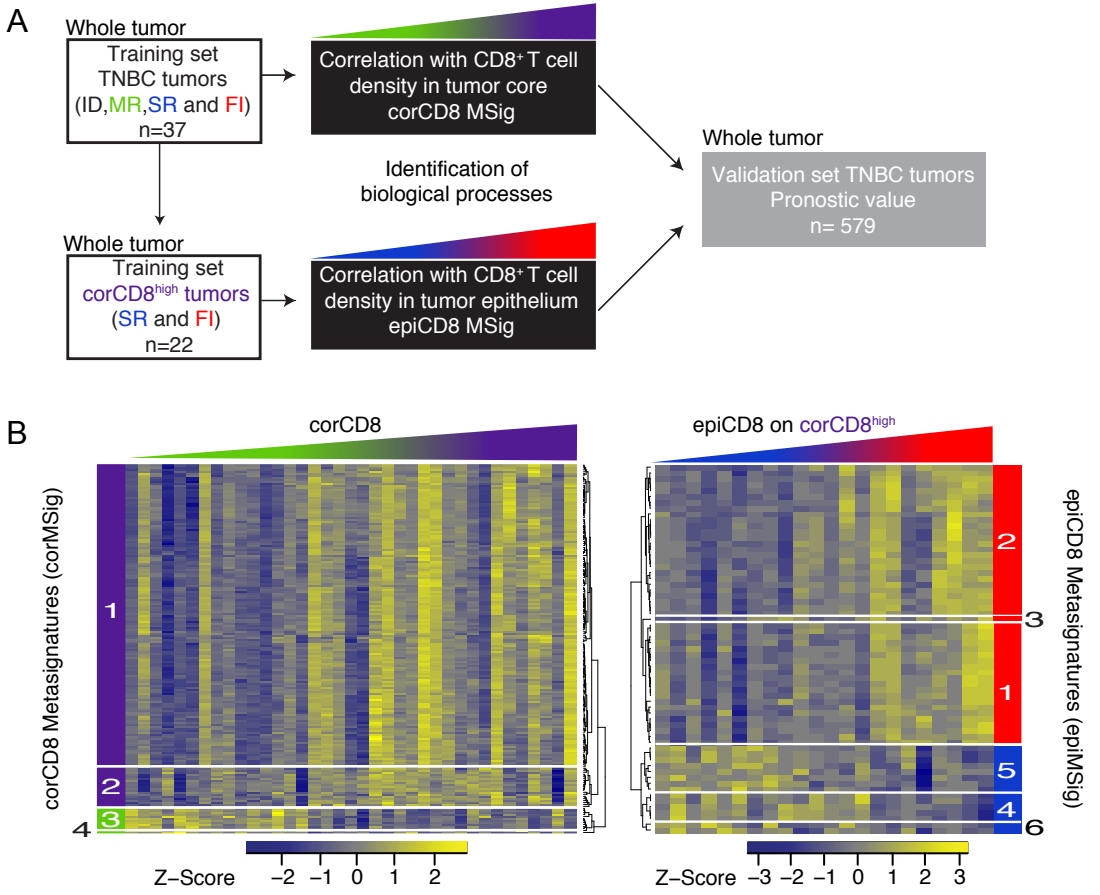


Figure 3. CD8+ T cell localization-derived Metasignature methodology. A) Analysis workflow for Metasignatures (MSig) and associated biological processes discovery in our dataset (n=37) and validation on external dataset (n=578). B) Left, clustering of pathway scores, derived from being positively or inversely correlated with CD8+ T cell density in tumor core (corCD8), identify 4 corCD8 Metasignatures (corCD8 MSig) in whole tumor gene expression of all TNBC tumors (n=37). Right, clustering of pathway scores, derived from being positively or inversely correlated with CD8+ T cell density in tumor epithelium (epiCD8), identify 6 epiCD8 Metasignatures (epiCD8 MSig). epiCD8 MSig are generated on the whole tumor gene expression of tumors showing CD8+ T cell infiltration in the tumor core (corCD8high, n=22, SR and FI tumors).

# Figure 4

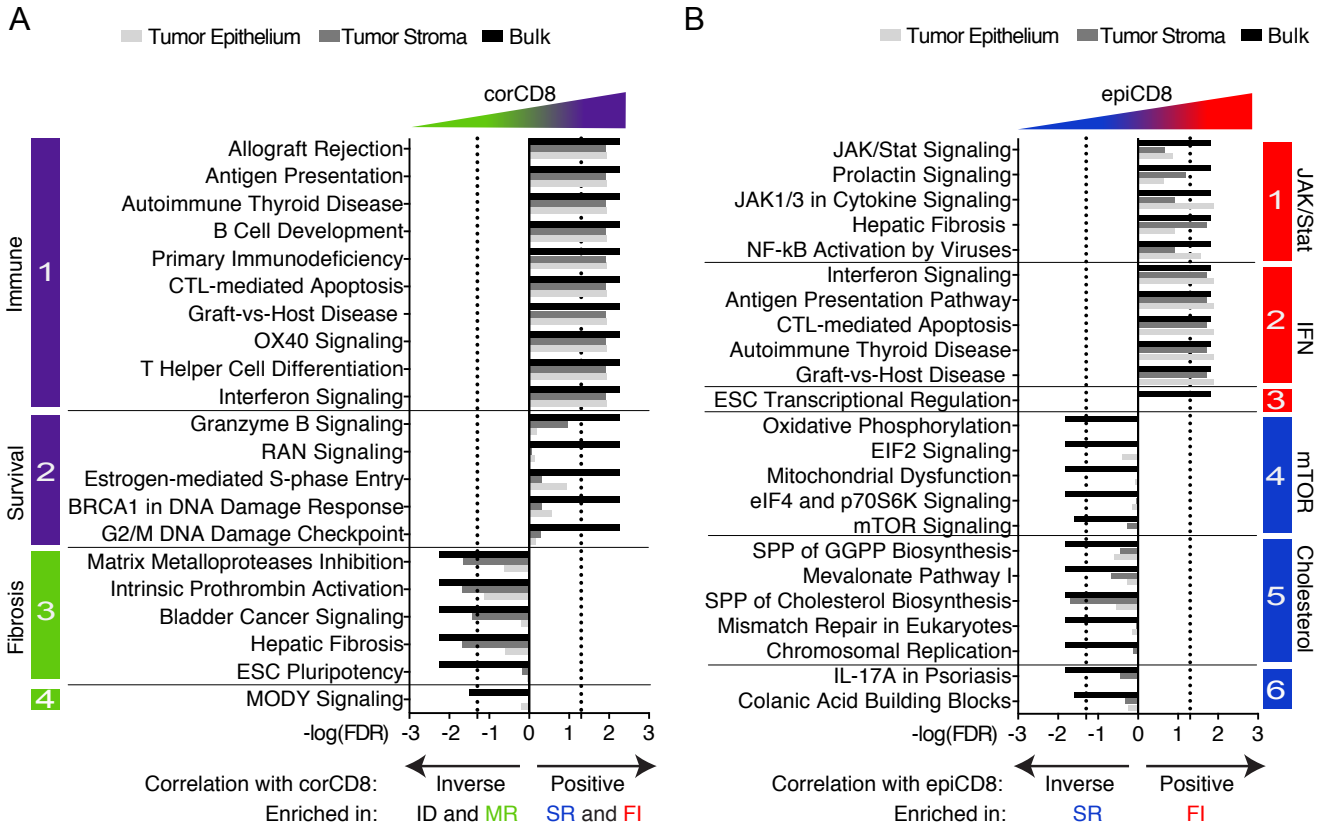


Figure 4. CD8⁺ T cell localization-derived Metasignatures identify distinct biological processes. A,B) Cellular pathways positively or inversely correlated with (A) CD8⁺ T cell density in the tumor core (corCD8) of all n=37 TNBC and (B) with CD8⁺ T cell density in the tumor epithelium (epiCD8) of n=22 TNBC corCD8$^{high}$ (SR and FI) tumors. Spearman correlation. Cellular pathway score FDR values are represented in whole tumor (black), tumor stroma (grey) and tumor epithelium (light grey). Top 5 significant pathways per Metasignature (MSig) are represented (except for corCD8 Msig1 for which the top10 pathways are represented to reflect the dominance of the MSig). MODY, Maturity Onset Diabetes of Young. CTL, Cytotoxic T Lymphocytes. SPP, Superpathway. ESC, Embryonic Stem Cells. Pathway names have been abbreviated. Full names of pathways can be found in Supplementary Tables 2 and 3.

# Figure 5

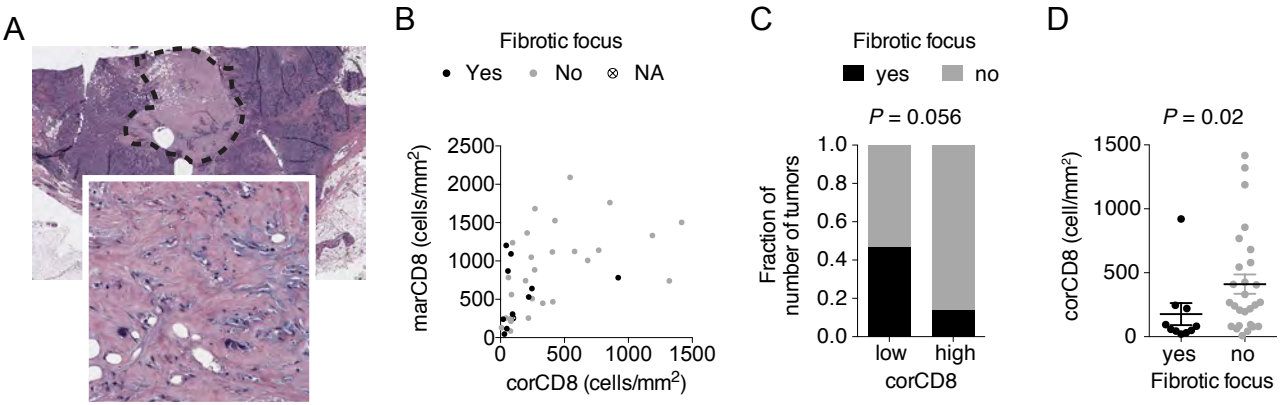


Figure 5. Tumors with poor infiltration of CD8⁺ T cells are enriched for fibrotic foci. A) Representative image of fibrotic focus on H&E stain. Image and zoom are 7x10mm and 0.5x0.5mm respectively. Dotted line identifies fibrotic focus. B) Fibrotic focus presence represented as 2D plot of marCD8 over corCD8 densities (n=38). C) Fibrotic focus presence is enriched in $corCD8^{low}$ compared to $corCD8^{high}$ tumors (n=38). Fischer Exact test. D) corCD8 is higher in tumors not containing fibrotic focus (n=38). Mann-Whitney test. Error bars, mean±SEM.

# Figure 6

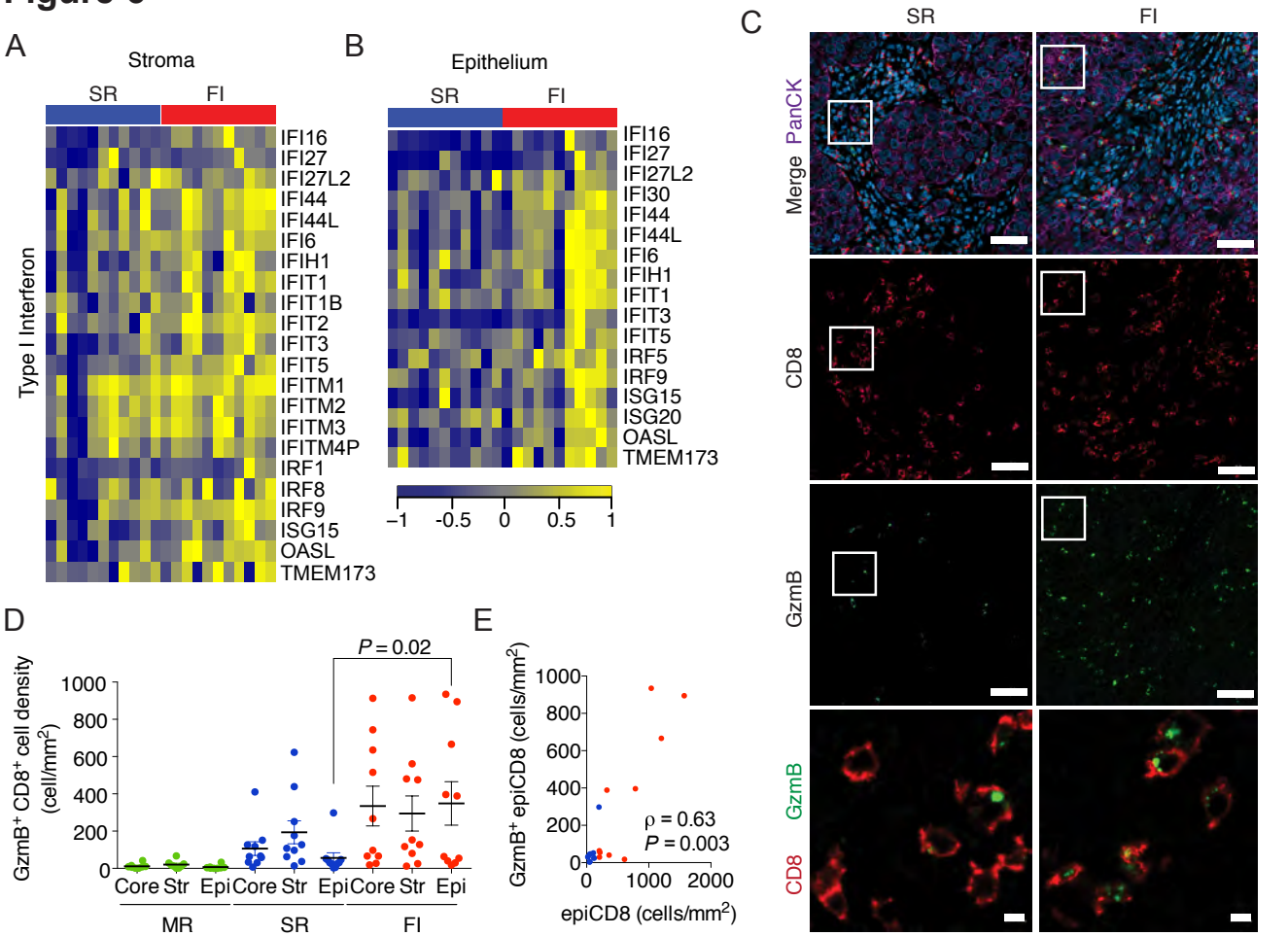


Figure 6. Fully inflamed TNBC are associated with a pro-inflammatory tumor immune microenvironment. A-B) Heatmap depicting expression of genes associated with a type I IFN response and cytotoxic activity in the tumor stroma (A) and epithelium (B) (n=22). C) Representative images showing a higher number of GzmB$^+$ CD8$^+$ T cells in FI tumor epithelium compared to SR. PanCK (pink) staining identifies tumor cells and DAPI (blue) the nuclei. White squares represent the position of zoomed in regions: stroma region for SR and epithelium region for FI. Scale for Merge, CD8 and GzmB is 50µm. Scale for CD8 GzmB colocalization is 5µm. n=22. D) Quantification of GzmB$^+$ CD8$^+$ T cells in tumor core, tumor stroma and tumor epithelium (n=32). Kruskal-Wallis test. Error bars, mean±SEM. E) GzmB$^+$ CD8$^+$ T cell density in tumor epithelium is positively correlated with epiCD8 (n=20). Spearman correlation. Green, blue and red dots represent ID, MR, SR and FI tumors respectively.

# Figure 7

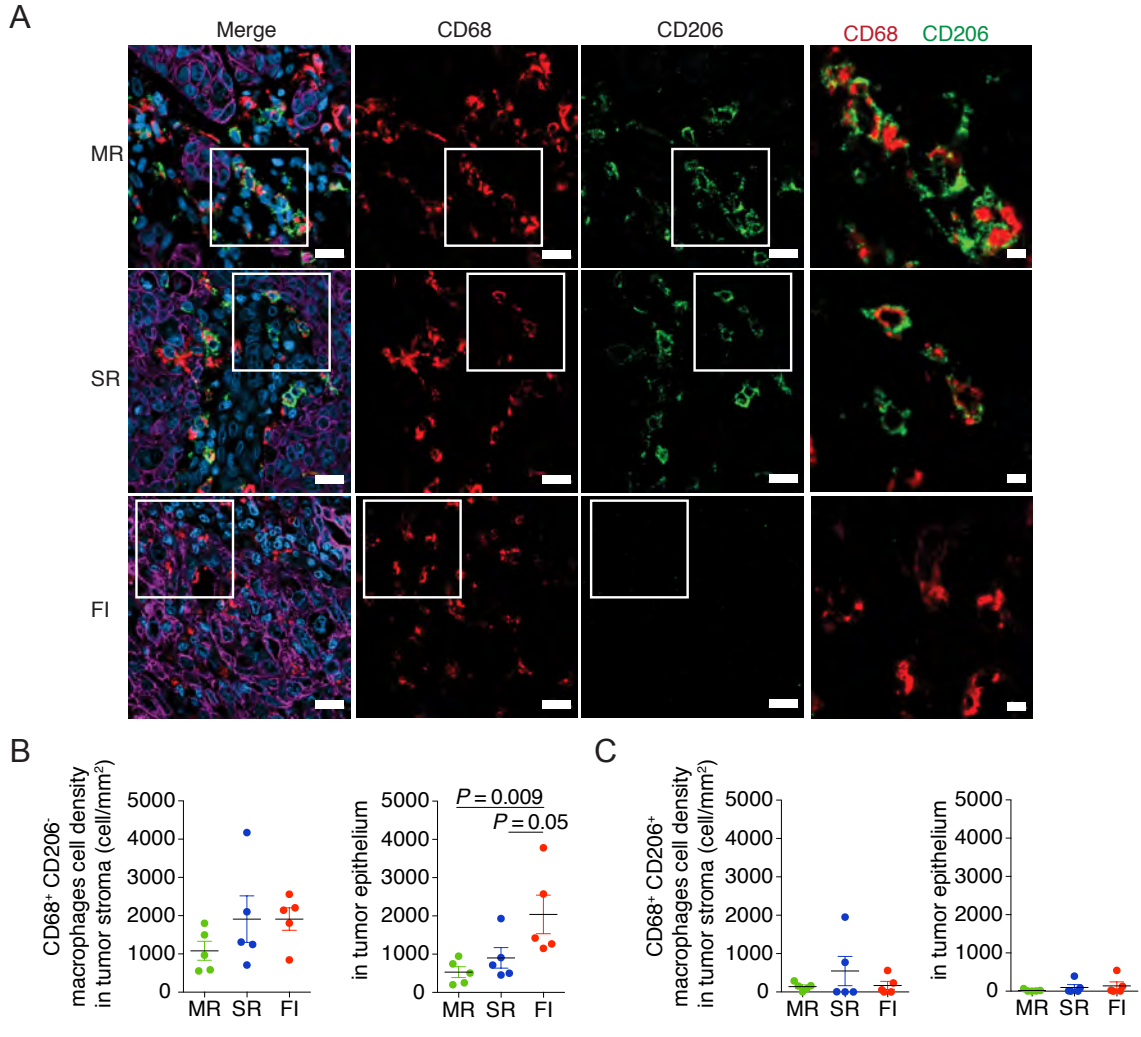


Figure 7. Fully inflamed TNBC are infiltrated with pro-inflammatory macrophages. A) Representative images of CD68$^{+}$ CD206$^{-}$ and CD68$^{+}$ CD206$^{+}$ macrophages show accumulation of pro-inflammatory CD68$^{+}$ CD206$^{-}$ in Fully inflamed (FI) tumors. n=15. White squares represent the position of zoomed in regions: stroma region for MR and SR and epithelium region for FI. PanCK (pink) identifies tumor cells and DAPI (blue) identifies cell nuclei. Merge, CD68, and CD206 scale is 50µm. CD68 and CD206 colocalization zoom scale is 5µm. B-C) Quantification of CD68$^{+}$ CD206$^{-}$ (B) and CD68$^{+}$ CD206$^{+}$ (C) macrophages in each tissue compartment across groups (n=15). Green, blue and red dots represent MR, SR and FI tumors respectively. Kruskal-Wallis test. Error bars, mean±SEM

# Figure 8

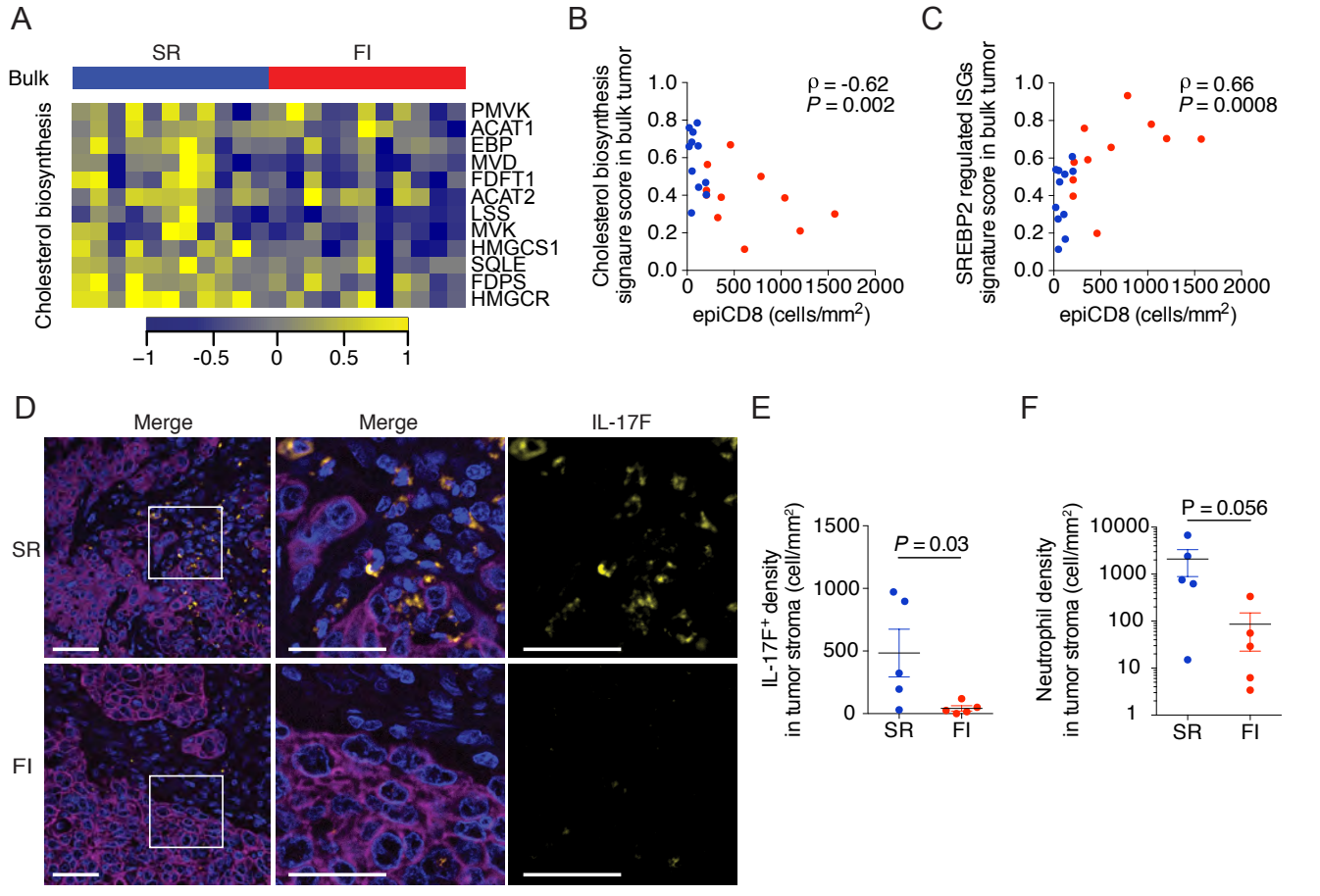


Figure 8. Stroma restricted TNBC are defined by a cholesterol gene expression signature and a distinct TIME. A) Heatmap depicting expression of genes of the superpathway of Cholesterol biosynthesis in bulk tumor in SR and FI tumors (n=22). B) Signature score of genes depicted in (A). Spearmann correlation. C) Signature score of Interferon Stimulated Genes (ISGs) repressed by SREBP2 showing decreased expression in SR compared to FI tumors (n=22). Spearman correlation. From Figure 2 are Stat=-0.67, *P*=0.02. D) Representative images of IHF depicting presence of IL-17-producing cells in the tumor stroma of SR versus FI tumors. Blue, DAPI. Pink, Pan-cytokeratin. Yellow, IL-17F. White squares represent position of zoomed in images. n=22. Merge and zooms scales are 50µm and 20µm respectively. E,F) IL-17-producing cell (E) and neutrophil (F) density across SR and FI tumors (n=10; 5 patients with the lowest and the highest epiCD8 respectively for SR and FI). Mann-Whitney test. Error bars, mean±SEM. Blue and red dots and bars represent SR and FI tumors respectively.

# Figure 9

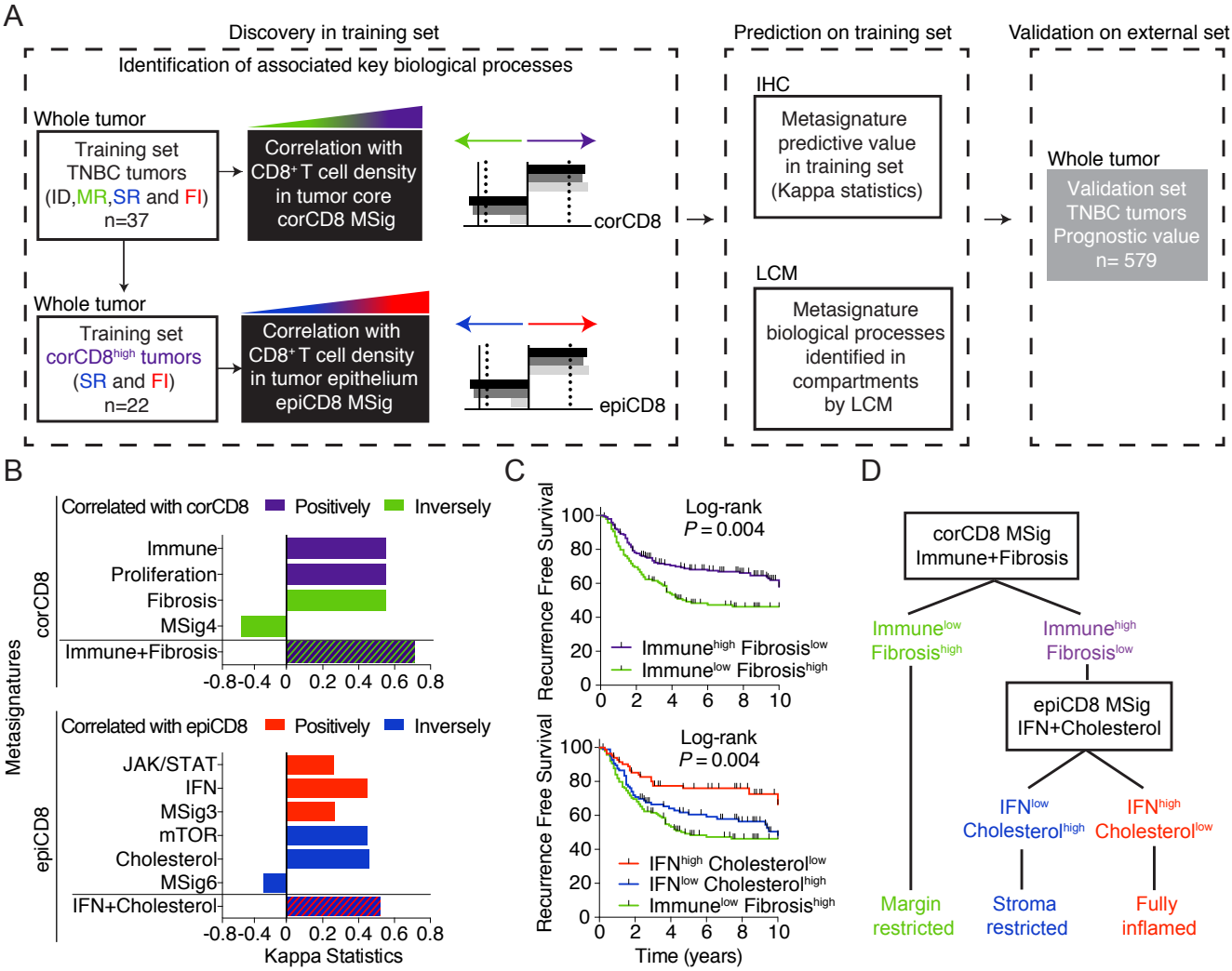


Figure 9. TIME Metasignatures show prognostic value in external TNBC cohort. A) Analysis pipeline showing (1) Discovery of metasignatures in 2-step process (corCD8 then epiCD8 stratification), (2) Prediction in our training set and (3) Validation on external set. B) Cohen's Kappa statistics measuring the prediction accuracy of each metasignature and combinations. C) Recurrence free survival curves using the identified combinations of corCD8 MSig (up; n=337) and epiCD8 MSig (down; n=196). For the corCD8 MSig Immune$^{High}$ Fibrosis$^{Low}$ vs. Immune$^{Low}$Fibrosis$^{High}$, the Hazard ratio is 0.63 [0.456, 0.887] $P$= 0.006. For the epiCD8 MSig IFN$^{High}$ Cholesterol$^{Low}$ vs. IFN$^{Low}$Cholesterol$^{High}$, the Hazard ratio is 0.52 [0.330, 0.843] $P$= 0.01. Log Rank test $P$ value is shown on the plots. D) Working model of TNBC stratification into immune subgroups based on the Metasignatures identified. MSig, Metasignature.

# Figure 10

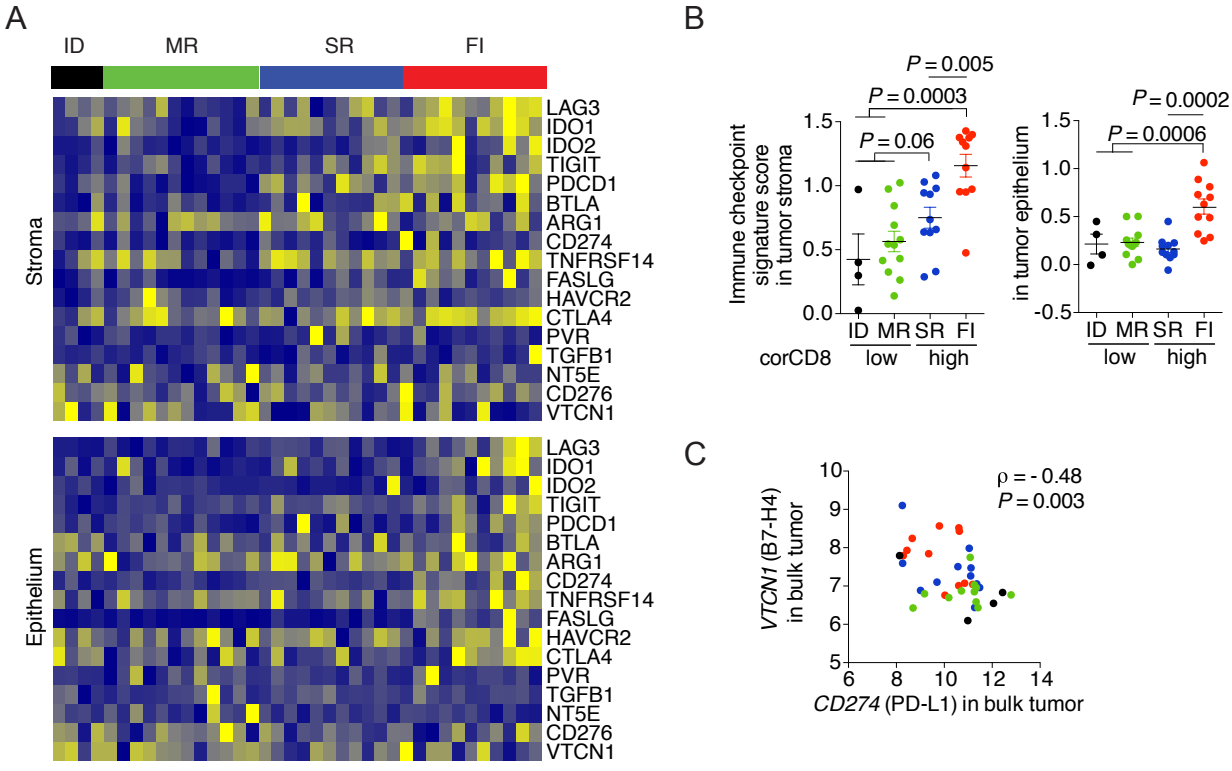


Figure 10. TIME TNBC subtypes express distinct markers of immune suppression. A) Heatmap depicting expression of classical immunosuppressive genes for each patient in tumor stroma (top) and epithelium (bottom) (n=38). B) Signature scores for the immunosuppressive gene list from (A) (n=38). Kruskal-Wallis test. Error bars, mean ± SEM. C) *VTCN1* (B7-H4) and *CD274* (PD-L1) gene expression are inversely correlated (n=37). Spearman correlation. Black, green, blue and red dots represent ID, MR, SR and FI tumors respectively.

# Figure 11

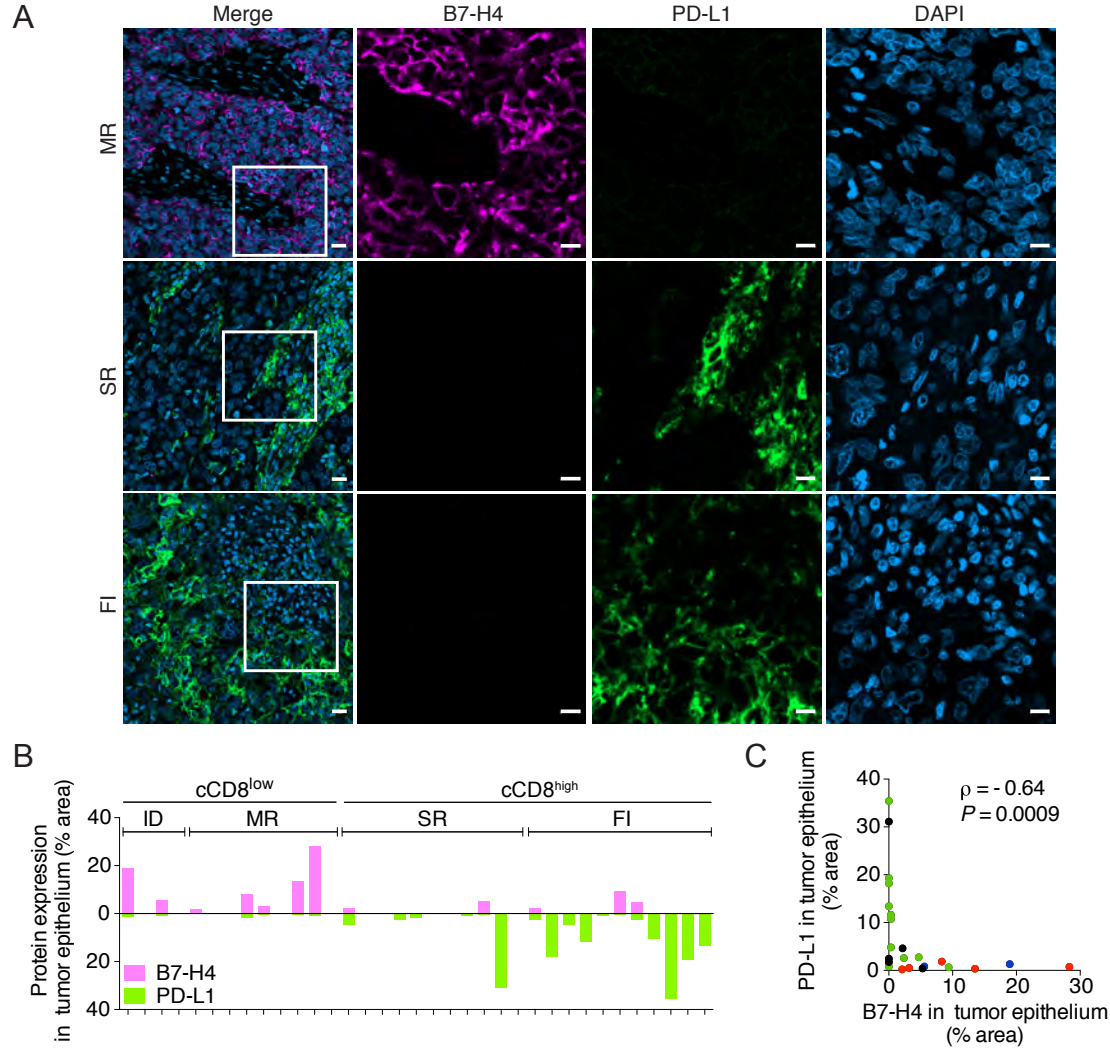


Figure 11. TIME TNBC subtypes display mutual exclusion and distinct localization of PD-L1 and B7-H4. A) Representative images of PD-L1 (green), B7-H4 (pink), and DAPI (blue) IHF stained sections. Image and zoom scales are 10µm and 20µm respectively. B) Quantification of staining in the tumor epithelium compartment for B7-H4 (pink) and PD-L1 (green) per patient (n=35). C) B7-H4 and PD-L1 quantifications after IHF show inverse correlation in the tumor epithelium compartment. This excludes tumors with <1% of stained epithelium compartment for both markers. Spearman correlation. Black, green, blue and red dots represent ID, MR, SR and FI tumors respectively.

# Figure 12

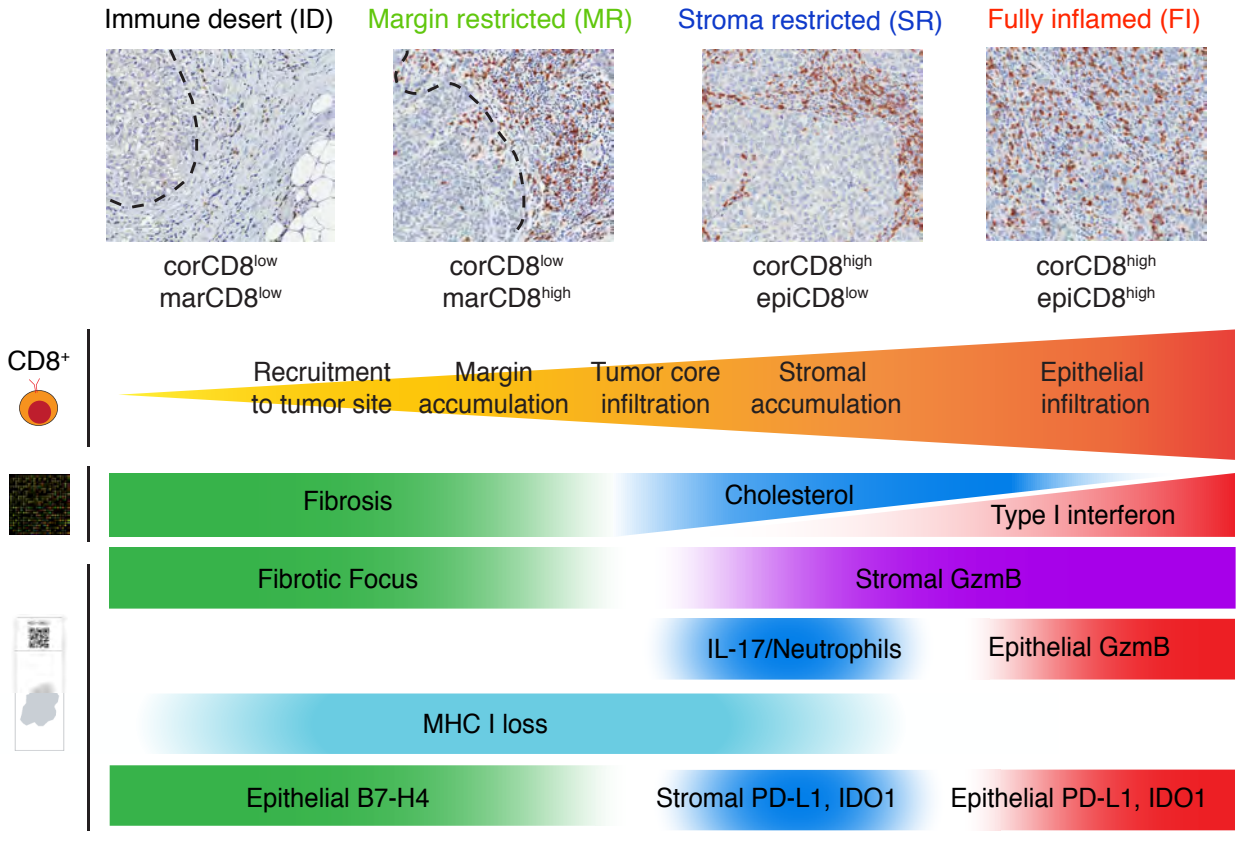


Figure 12. Schematic of TIME TNBC subtype stratification. Poorly infiltrated tumors (Immune desert and Margin restricted) are characterized by signature of fibrosis, enrichment of fibrotic foci and expression of the immune checkpoint B7-H4. Tumors that display significant infiltration of CD8+ T cells in the tumor core but that specifically accumulate in the tumor stroma display signatures of cholesterol, infiltration of IL-17-producing cells and neutrophils. MHC I depletion can be found in tumors from all TIME subtypes except FI. Those tumors also display stromal expression of the immune checkpoint PD-L1. Tumors with significant infiltration in the tumor core and in the tumor epithelium are characterized by Type I interferon signatures as well as activated CD8+ T cell (GzmB+) and PD-L1 expression in the tumor epithelium compartment. GzmB, Granzyme B. ID, Immune desert ; MR, Margin restricted ; SR Stroma restricted ; FI, Fully inflamed.